

Effects of spin viscosity on ferrofluid flow profiles in alternating and rotating magnetic fields

Carlos Rinaldi

Department of Chemical Engineering, Massachusetts Institute of Technology, 77 Massachusetts Avenue, Cambridge, Massachusetts 02139

Markus Zahn

Department of Electrical Engineering and Computer Science, Massachusetts Institute of Technology, 77 Massachusetts Avenue, Cambridge, Massachusetts 02139

(Received 10 September 2001; accepted 23 April 2002; published 3 July 2002)

Previous models of plane-Poiseuille flow of ferrofluids in alternating and rotating magnetic fields are extended by including the effects of spin diffusion and planar Couette flow. Accurate modeling of this problem is required for the design of experiments to determine key parameters for previously reported anomalous forward and backward ferrofluid pumping behavior in alternating and rotating magnetic fields. The previously derived zero-spin-viscosity analysis predicted multi-valued and singular flow solutions with possible zero and negative effective magnetoviscosity. This analysis calculates analytical expressions for the translational and spin velocity profiles, vorticity profiles, volumetric flow rate, and the shear force on a moving duct surface, comparing the effects of boundary conditions of zero spin velocity and spin velocity equal to half the vorticity at the duct walls. The analysis shows that the single singularity in flow behavior corresponding to zero magnetoviscosity in the zero-spin-viscosity analysis expands to multiple possible flow singularities for the nonzero spin viscosity case. Simple representative shearing experiments are proposed to differentiate between the zero and nonzero spin viscosity solutions, to calculate the values of key viscous parameters, and to show how wall boundary conditions can be determined from shear stress measurements. © 2002 American Institute of Physics. [DOI: 10.1063/1.1485762]

I. BACKGROUND

Recent analyses and measurements have shown anomalous behavior of ferrofluids in ac magnetic fields, whereby in linearly polarized or rotating magnetic fields the effective fluid viscosity can be increased or decreased and the flow direction can reverse against a pressure gradient as a function of magnetic field amplitude, frequency, and direction.¹⁻⁹ This anomalous behavior can be explained using the governing fluid mechanical linear and angular momentum conservation equations including a nonsymmetric viscous stress tensor. Past work along these lines has taken the spin viscosity to be zero.⁷⁻⁹ This work extends this past plane Poiseuille ferrofluid flow analysis by examining the effects of nonzero spin viscosity, different spin boundary conditions, and including the effect of relative motion of the parallel plates (Couette flow).

We examine simple cases where the applied magnetic fields along and transverse to a duct axis are spatially uniform and vary sinusoidally with time with either linear or elliptical polarizations. In the uniform magnetic field, the magnetization characteristic depends on fluid spin velocity but does not depend on fluid flow velocity. The magnetization force density along the duct axis is then zero while the magnetic torque density is nonzero as magnetization and magnetic fields are not collinear due to Brownian and Néel magnetic relaxation processes as well as due to the effects of fluid spin.

A. Governing equations

1. Linear and internal angular momentum equations

The basic equations governing ferrofluid flow are the linear and internal angular momentum equations,¹⁰⁻¹³ and the magnetization equation.^{2,14} The linear momentum equation for structured continua is derived from a macroscopic linear momentum conservation statement and takes the form¹¹

$$\rho \frac{D\mathbf{v}}{Dt} = \nabla \cdot \mathbf{T} + \mathbf{f}, \quad (1.1)$$

where ρ is the mass density of the ferrofluid, \mathbf{v} the mass-average velocity, \mathbf{T} the Cauchy stress tensor representing the effect of short-range “push-pull-shear” forces, such as pressure and viscous forces, and \mathbf{f} the body-force density field, representing the effects of long-range “action-at-a-distance” forces, such as gravity and magnetization forces. Equation (1.1) is written in terms of the convected or “Lagrangian” derivative of fluid mechanics,

$$\frac{D}{Dt} = \frac{\partial}{\partial t} + \mathbf{v} \cdot \nabla, \quad (1.2)$$

where $\partial/\partial t$ denotes the local or “Eulerian” temporal rate of change.

The internal angular momentum equation is similarly derived from a macroscopic angular momentum conservation

statement, coupled with the moment of the linear momentum equation. The resulting governing equation for isotropic spherical particles is¹¹

$$\rho\kappa \frac{D\boldsymbol{\omega}}{Dt} = \nabla \cdot \mathbf{C} + \mathbf{T}_\times + \mathbf{I}, \tag{1.3}$$

where κ is a scalar moment-of-inertia density, $\boldsymbol{\omega}$ is the so-called spin-velocity of the suspension, \mathbf{C} the couple stress dyadic, representing the effect of the short-range transport of intrinsic angular momentum, \mathbf{T}_\times the antisymmetric vector of the Cauchy stress ($\mathbf{T}_\times = -\boldsymbol{\epsilon} : \mathbf{T}$, where $\boldsymbol{\epsilon}$ is the unit pseudo-isotropic triadic), and \mathbf{I} is the body-couple density field, representing the effect of the “long-range” transport of intrinsic angular momentum. An important implicit assumption in the linear and internal angular momentum equations as written here is that the polarized substructure behaves as a rigid body, meaning the magnetic particles comprising the ferrofluid are supposed to behave as rigid particles.

2. Magnetization equation

The magnetization equation is a phenomenological equation describing the behavior of magnetic particles suspended in a nonmagnetic medium. The magnetization vector \mathbf{M} of the particles, in the Eulerian frame, changes according to the following equation:¹⁵

$$\frac{\partial \mathbf{M}}{\partial t} + \nabla \cdot (\mathbf{v}\mathbf{M}) = \boldsymbol{\omega} \times \mathbf{M} - \frac{1}{\tau} (\mathbf{M} - \mathbf{M}_{eq}), \tag{1.4}$$

where the first term on the right-hand side represents changes in magnetization due to “rotation” of the magnetized particles¹⁶ and the second term represents change in magnetization towards an “equilibrium” magnetization \mathbf{M}_{eq} via various “relaxation” processes, with combined time constant τ . Equation (1.4) reduces to the form given by Rosensweig (1997)¹⁴ for an incompressible ferrofluid. The second term on the left-hand side properly accounts for the convective flux of the per-unit-volume material property \mathbf{M} .

The commonly accepted relaxation processes for practical ferrofluid suspensions are rotational Brownian motion, with characteristic time constant

$$\tau_B = 3V_p \frac{\eta_0}{kT}, \tag{1.5}$$

and Néel relaxation, with characteristic time constant

$$\tau_N = \frac{1}{f_0} \exp\left(\frac{K_a V_p}{kT}\right), \tag{1.6}$$

where V_p is the magnetic particle’s volume, η_0 is the viscosity of the carrier fluid, $k \sim 1.38 \times 10^{-23} \text{ JK}^{-1}$ is Boltzmann’s constant, T is the temperature in degrees Kelvin, K_a is the anisotropy constant of the single-domain uniaxial ferromagnetic particle, and f_0 is a normalization frequency.¹⁴ In Brownian motion the particle magnetic moment is fixed to the particle and tries to align with the local magnetic field by particle rotation, while for Néel relaxation the particle magnetic moment rotates to align with the local magnetic field without particle rotation (through rearrange-

ment of the magnetic domains in the particle). The relaxation time constant τ in (1.4) is related to the Brownian and Néel time constants as

$$\frac{1}{\tau} = \frac{1}{\tau_B} + \frac{1}{\tau_N}. \tag{1.7}$$

We have performed preliminary viscosity measurements with IsoparM based ferrofluid ($\eta_0 = 0.03 \text{ Nm}^{-2}\text{s}$) using magnetite particles with diameters of order 8–16 nm. For this ferrofluid (1.5) and (1.6) predict that $\tau_B \sim 5 \times 10^{-6} - 5 \times 10^{-5} \text{ s}$ and $\tau_N \sim 4 \times 10^{-9} - 2 \times 10^{-4} \text{ s}$ (at 300 K and using¹⁴ $f_0 = 10^9 \text{ Hz}$ and $K_a = 23,000 \text{ Jm}^{-3}$). For a sample IsoparM ferrofluid with particle diameters of 15 nm the combined relaxation time constant is then $\tau \sim 10^{-5} \text{ s}$ [using (1.5)–(1.7)]. This value for the relaxation time constant will be used as a representative value in all subsequent calculations.

3. Constitutive equations

Constitutive equations are required for the dynamical quantities \mathbf{f} and \mathbf{I} , the rheological quantities \mathbf{T} and \mathbf{C} , as well as for the equilibrium magnetization \mathbf{M}_{eq} . For incompressible ferrofluids, the body-force density is composed of magnetic and gravitational contributions and takes the form¹⁴

$$\mathbf{f} = \rho\mathbf{g} + \mu_0 \mathbf{M} \cdot \nabla \mathbf{H}, \tag{1.8}$$

where \mathbf{g} is the gravitational field vector, $\mu_0 (= 4\pi \times 10^{-7} \text{ Henries/meter})$ is the permeability of free space, and \mathbf{H} is the magnetic field in the suspension. Should the magnetic fluid be compressible, magnetostriction terms would also be present in (1.8),¹⁴ but in the analysis treated in this paper we assume that the magnetic fluid is incompressible. The body-couple density is commonly assumed to consist solely of a magnetic contribution, and takes the form

$$\mathbf{I} = \mu_0 \mathbf{M} \times \mathbf{H}. \tag{1.9}$$

However, we note that for particles with an anisotropic mass distribution a gravitational body-couple will result in general.^{17,18} We choose to neglect these effects here.

From a rheological standpoint, ferrofluid suspensions are interesting in that they are a commercially relevant example of systems characterized by an asymmetric state of stress at the suspension scale. Thus, in its simplest form, the Cauchy stress field is described by a symmetric component, commonly described by a Newtonian model, as well as an anti-symmetric component representing transport of angular momentum between the internal and external modes,^{11,12,14}

$$\mathbf{T} = -p\mathbf{I} + \eta[\nabla \mathbf{v} + \nabla \mathbf{v}^T] + \lambda(\nabla \cdot \mathbf{v})\mathbf{I} + \zeta \boldsymbol{\epsilon} \cdot (\nabla \times \mathbf{v} - 2\boldsymbol{\omega}), \tag{1.10}$$

where \mathbf{I} is the idemfactor (unit isotropic dyadic), the term p represents the hydrostatic pressure contribution, and η , λ , and ζ are the coefficients of shear, bulk, and vortex viscosity, respectively.

Ferrofluid suspensions are also interesting because the diffusive transport of internal angular momentum may contribute to the flow behavior. This effect is described by the couple stress dyadic \mathbf{C} , commonly given the constitutive form¹⁹

$$\mathbf{C} = \eta' [\nabla \boldsymbol{\omega} + \nabla \boldsymbol{\omega}^T] + \lambda' (\nabla \cdot \boldsymbol{\omega}) \mathbf{I}, \quad (1.11)$$

where η' and λ' are the shear and bulk coefficients of spin viscosity. The coefficients η , λ , ζ , η' , and λ' are required to be positive, in accordance with the Second Law of Thermodynamics.²⁰

The equilibrium magnetization vector is generally described by the Langevin equation. In the low magnetic field limit, the magnetization is approximately linear with H , with constant magnetic susceptibility χ_0 .

$$\mathbf{M}_{\text{eq}} = \chi_0 \mathbf{H}, \quad (1.12)$$

where χ_0 is, in general, dependent on suspension composition and temperature, as well as particle and suspending fluid properties. This relation is given explicitly for weakly interacting particles by¹⁴

$$\chi_0 = \frac{1}{3} \frac{\phi \mu_0 M_p^2 V_p}{kT}, \quad (1.13)$$

where ϕ is the volume fraction of magnetic particles and M_p is the magnitude of the particle-locked magnetic dipole moment density. This low magnetization limit is appropriate when the Langevin parameter α_L is much less than unity¹⁴

$$\alpha_L = \frac{\mu_0 M_p H V_p}{kT} \ll 1. \quad (1.14)$$

In essence, this requirement provides a maximum applied magnetic field for which (1.12) is applicable.

As the magnetic field increases, more of the magnetic particles align with the field until the magnetization vector asymptotes to a saturation value corresponding to having all the body-locked magnetic dipoles collinear with the field. This magnetically saturated limit is given by a relationship of the form

$$\mathbf{M}_s = \phi M_p \mathbf{i}_H, \quad (1.15)$$

where \mathbf{i}_H is a unit vector in the direction of the magnetic field \mathbf{H} . For suspensions with polydisperse M_p a suitable ensemble average is required in (1.15).

For the IsoparM based ferrofluid with magnetite particles ($M_p = 4.46 \times 10^5 \text{ Am}^{-1}$)¹⁴ and diameters ranging from 8–16 nm, the magnetic susceptibility at room temperature predicted by (1.13) varies from 0.5–4.3. For this particular ferrofluid with particle diameter of 15 nm, (1.13) yields $\chi_0 \sim 3.5$ and (1.14) yields $\mu_0 H \ll 52 \text{ G}$ as the criterion of applicability of (1.12). These representative values will be used subsequently in our sample calculations.

4. Coupled translational velocity, spin velocity and magnetization equations

Introducing the constitutive relations embodied in (1.8)–(1.12) into the governing equations (1.1)–(1.4), we obtain

$$\begin{aligned} \rho \frac{D\mathbf{v}}{Dt} = & -\nabla p' + \mu_0 \mathbf{M} \cdot \nabla \mathbf{H} + 2\zeta \nabla \times \boldsymbol{\omega} + (\eta + \lambda - \zeta) \nabla \nabla \cdot \mathbf{v} \\ & + (\eta + \zeta) \nabla^2 \mathbf{v}, \end{aligned} \quad (1.16)$$

$$\begin{aligned} \rho \kappa \frac{D\boldsymbol{\omega}}{Dt} = & \mu_0 \mathbf{M} \times \mathbf{H} + 2\zeta (\nabla \times \mathbf{v} - 2\boldsymbol{\omega}) + (\eta' + \lambda') \nabla \nabla \cdot \boldsymbol{\omega} \\ & + \eta' \nabla^2 \boldsymbol{\omega}, \end{aligned} \quad (1.17)$$

$$\frac{\partial \mathbf{M}}{\partial t} + \nabla \cdot (\mathbf{v} \mathbf{M}) = \boldsymbol{\omega} \times \mathbf{M} - \frac{1}{\tau} (\mathbf{M} - \chi_0 \mathbf{H}), \quad (1.18)$$

where we have absorbed the gravitational force contribution into the dynamical pressure,²¹

$$p' = p - \rho(\mathbf{r} \cdot \mathbf{g}), \quad (1.19)$$

with \mathbf{r} a position vector with respect to an arbitrary origin O . This is appropriate for flows with constant mass density ρ and gravitational field \mathbf{g} . These three vector equations, in addition to the continuity equation, govern the dynamical behavior of isothermal ferrofluids.

5. Boundary conditions

In principle, all that is required to solve (1.16)–(1.18) for a given flow situation is a complete set of boundary conditions. The linear momentum equation requires an initial condition and two vector boundary conditions, commonly accepted to be the same as in classical fluid mechanics, i.e., the no-penetration and no slip boundary conditions:

$$\mathbf{n} \cdot \|\mathbf{v}\| = 0, \quad (1.20a)$$

$$\mathbf{n} \times \|\mathbf{v}\| = 0, \quad (1.20b)$$

where \mathbf{n} is the unit vector normal to the boundary in question and $\|\mathbf{v}\|$ represents the jump in the mass average velocity across the boundary. We note that previous studies have shown that slip velocities inversely proportional to a “friction coefficient” are possible in flowing suspensions.²² This is equivalent to Lamb’s²³ classical assumption that slip would be opposed by a tangential force. However, as the slip “friction coefficient” is inversely proportional to particle radius, these effects should be negligible in ferrofluid flows. Other work²⁴ has independently shown that such slip velocity effects are of the order of the ratio of particle and macroscopic linear dimensions [$O(l/L)$ with l the characteristic particle radius and L the characteristic macroscopic linear dimension of the system]. As such we neglect translational slip effects and choose to apply (1.20) as the boundary condition for the translational velocity field.

As with the translational velocity field, the equation describing spin requires an initial condition, as well as two vector boundary conditions. The appropriate boundary conditions for the spin field, on the other hand, are still a subject of debate.^{19,25–29} However, because most analyses of ferrofluid behavior neglect the effect of “spin-diffusion” by setting $\eta' = \lambda' = 0$, thereby reducing the second-order internal angular momentum equation, (1.17), to zero order and thus not requiring any boundary conditions on the spin field, $\boldsymbol{\omega}$, the spin-boundary condition has not received as much attention as the translational velocity boundary condition. Various possibilities are imaginable, depending on assumptions for the particle/wall interaction effects. In this contribution we

analyze two of these possibilities: (i) The “spin–no-slip” boundary condition and (ii) spin–vorticity matching at surfaces. Spin–no-slip:

$$\mathbf{n} \cdot \|\boldsymbol{\omega}\| = 0, \tag{1.21a}$$

$$\mathbf{n} \times \|\boldsymbol{\omega}\| = 0, \tag{1.21b}$$

corresponds to the assumption that particle/wall interactions are so strong that no relative spin between the two is possible.^{19,28} Spin/vorticity matching:

$$\|\boldsymbol{\omega} - \frac{1}{2} \nabla \times \mathbf{v}\| = 0, \tag{1.22}$$

corresponds to the assumption that antisymmetric stresses vanish at the wall.^{19,28} A linear combination of these boundary conditions is possible and is discussed in Aero *et al.*²⁸

B. Scaling of the governing equations

Practical application of the governing equations embodied in (1.16)–(1.18) generally requires substantial simplification based either on symmetry arguments, to reduce the number of equations and eliminate terms identically, or on scaling, to eliminate terms asymptotically.²¹ Here we focus on scaling of the equations. The objective is to make the magnitude of all nondimensional variables and their spatial and temporal derivatives of order unity. A series of dimensionless parameters are defined in the process, which upon comparison suggest which terms could be neglected for a given problem.

In this section, we have chosen to scale the spatial dimension differently in (1.16), (1.17), and (1.18) to emphasize the possibility that the field variables of interest (\mathbf{v} , $\boldsymbol{\omega}$, and \mathbf{M}) may in principle vary over widely different length scales (L_v for the characteristic length scale of velocity variations, L_ω for variations in spin velocity and L_M for variations in the magnetization field). Subsequently in the analysis of Secs. II and III we will assume that all three spatial scales are equal ($L_v = L_\omega = L_M$) and use the decorative symbol (\sim) to denote a field variable which has been properly scaled with respect to its magnitude.³⁰

1. Scaled linear momentum equation

The scaled linear-momentum equation (1.16) is

$$\begin{aligned} \text{Re} \left(\frac{1}{\text{Sr}} \frac{\partial \tilde{\mathbf{v}}}{\partial \hat{t}} + \tilde{\mathbf{v}} \cdot \tilde{\nabla} \tilde{\mathbf{v}} \right) \\ = - \left(\frac{\Pi' L_v}{\eta U} \right) \tilde{\nabla} \tilde{p}' + \left(\frac{\mu_0 M H L_v}{\eta U} \right) \tilde{\mathbf{M}} \cdot \tilde{\nabla} \tilde{\mathbf{H}} + 2 \left(\frac{\Omega L_v \zeta}{U \eta} \right) \\ \times \tilde{\nabla} \times \tilde{\boldsymbol{\omega}} + \frac{(\lambda + \eta - \zeta)}{\eta} \tilde{\nabla} \tilde{\nabla} \cdot \tilde{\mathbf{v}} + \left(1 + \frac{\zeta}{\eta} \right) \tilde{\nabla}^2 \tilde{\mathbf{v}}, \end{aligned} \tag{1.23}$$

where U is the scale of the translational velocity, L_v is the characteristic length scale for spatial variations in \mathbf{v} , Π' is the scale of the dynamical pressure field, M is the magnitude of the magnetization vector, H is the scale of the magnetic field vector, and Ω is the scale of the spin field. All quantities with a (\sim) are “scaled” quantities assumed to be of order unity.³¹ This is, of course, subject to *a posteriori* verification

when solving a given problem. Explicitly, the scaled quantities in (1.23) are related to the original quantities in (1.16) by

$$\begin{aligned} \tilde{\mathbf{v}} = \mathbf{v}/U, \quad \tilde{\nabla} = L_v \nabla, \quad \tilde{p}' = p'/\Pi', \quad \tilde{\mathbf{M}} = \mathbf{M}/M, \\ \tilde{\mathbf{H}} = \mathbf{H}/H, \quad \tilde{\boldsymbol{\omega}} = \boldsymbol{\omega}/\Omega, \quad \tilde{t} = t/\tau_v. \end{aligned} \tag{1.24}$$

We have introduced two well known dimensionless factors in (1.23): the Reynolds number,

$$\text{Re} = \frac{\rho U L_v}{\eta}, \tag{1.25}$$

representing the relative magnitudes of diffusive, $\eta U/L_v^2$, and convective, $\rho U^2/L_v$, momentum transfer, and the Strouhal number,

$$\text{Sr} = \frac{U \tau_v}{L_v}, \tag{1.26}$$

representing the relative magnitudes of the convective time scale, L_v/U , and the characteristic time of velocity variations, τ_v .²¹

2. Scaled internal angular momentum equation

The internal angular momentum equation, (1.17), may be similarly scaled. The result is

$$\begin{aligned} \text{Re}_\omega \left(\frac{1}{\text{Sr}_\omega} \frac{\partial \tilde{\boldsymbol{\omega}}}{\partial \hat{t}} + \tilde{\mathbf{v}} \cdot \tilde{\nabla} \tilde{\boldsymbol{\omega}} \right) \\ = \left(\frac{\mu_0 M H L_\omega^2}{\eta' \Omega} \right) \tilde{\mathbf{M}} \times \tilde{\mathbf{H}} + 2 \left(\frac{\zeta L_\omega^2}{\eta'} \right) \left(\frac{U}{\Omega L_\omega} \tilde{\nabla} \times \tilde{\mathbf{v}} - 2 \tilde{\boldsymbol{\omega}} \right) \\ + \frac{(\eta' + \lambda')}{\eta'} \tilde{\nabla} \tilde{\nabla} \cdot \tilde{\boldsymbol{\omega}} + \hat{\nabla}^2 \tilde{\boldsymbol{\omega}}, \end{aligned} \tag{1.27}$$

where L_ω is the characteristic length scale for spatial variations in the spin $\boldsymbol{\omega}$.³² Two new scaled quantities have been introduced in these equations, $\hat{\nabla}$ and \hat{t} . These are related to the original quantities in (1.17) by

$$\hat{\nabla} = L_\omega \nabla, \quad \hat{t} = t/\tau_\omega, \tag{1.28}$$

with τ_ω the characteristic time scale for changes in the spin velocity. We have also defined two new quantities, directly analogous to the Reynolds and Strouhal numbers. These are the spin-Reynolds number,

$$\begin{aligned} \text{Re}_\omega = \rho \kappa \frac{U L_\omega}{\eta'} \\ = \left(\frac{L_\omega}{L_v} \right) \left(\frac{\kappa \eta}{\eta'} \right) \text{Re}, \end{aligned} \tag{1.29}$$

representing the relative magnitudes of diffusive, $\eta' \Omega/L_\omega^2$, and convective, $\rho \kappa \Omega U/L_\omega$, transport of internal angular momentum, and the spin-Strouhal number,

$$\begin{aligned} \text{Sr}_\omega = \frac{U \tau_\omega}{L_\omega} \\ = \left(\frac{L_v}{L_\omega} \right) \left(\frac{\tau_\omega}{\tau_v} \right) \text{Sr}, \end{aligned} \tag{1.30}$$

representing the relative magnitudes of the convective time scale, L_ω/U , and the characteristic time for spin variations, τ_ω .

3. Scaled magnetization equation

Finally, the magnetization equation may be similarly scaled, resulting in

$$\frac{1}{\tau_M} \frac{\partial \tilde{\mathbf{M}}}{\partial \tilde{t}} + \frac{U}{L_M} \tilde{\nabla} \cdot (\mathbf{v} \tilde{\mathbf{M}}) = \Omega \tilde{\omega} \times \tilde{\mathbf{M}} - \frac{1}{\tau} \left(\tilde{\mathbf{M}} - \frac{\chi_0 H}{M} \tilde{\mathbf{H}} \right), \tag{1.31}$$

where τ_M is a characteristic time for variations in magnetization, L_M is the characteristic length scale for changes in the magnetization vector (L_M/U is a characteristic time scale for convection of magnetization), and Ω^{-1} acts as a time scale for changes due to the rotation of the magnetization vector via the spin velocity. The scaled quantities $\tilde{\nabla}$ and \tilde{t} are related to the original quantities in (1.18) by

$$\tilde{\nabla} = L_M \nabla, \quad \tilde{t} = t/\tau_M. \tag{1.32}$$

4. Incompressible creeping-flow limit of the translational and spin-velocity equations

Here we introduce the simplifying assumption that the ferrofluid is incompressible, hence $\nabla \cdot \mathbf{v} = 0$ exactly. Creeping flow in the translational and spin velocities is approached asymptotically as the translational and spin-Reynolds numbers approach zero ($\text{Re} \rightarrow 0, \text{Re}_\omega \rightarrow 0$). In this limit, the linear and internal angular momentum equations reduce to

$$0 = - \left(\frac{\Pi' L_v}{\eta U} \right) \tilde{\nabla} \tilde{p}' + \left(\frac{\mu_0 M H L_v}{\eta U} \right) \tilde{\mathbf{M}} \cdot \tilde{\nabla} \tilde{\mathbf{H}} + 2 \left(\frac{\zeta \Omega L_v}{\eta U} \right) \tilde{\nabla} \times \tilde{\omega} + \left(1 + \frac{\zeta}{\eta} \right) \tilde{\nabla}^2 \tilde{\mathbf{v}}, \tag{1.33}$$

and

$$0 = \left(\frac{\mu_0 M H L_\omega^2}{\eta' \Omega} \right) \tilde{\mathbf{M}} \times \tilde{\mathbf{H}} + 2 \frac{\zeta}{\eta'} \frac{L_\omega U}{\Omega} \tilde{\nabla} \times \tilde{\mathbf{v}} - 4 \left(\frac{\zeta L_\omega^2}{\eta'} \right) \tilde{\omega} + \frac{(\eta' + \lambda')}{\eta'} \tilde{\nabla} \tilde{\nabla} \cdot \tilde{\omega} + \tilde{\nabla}^2 \tilde{\omega}, \tag{1.34}$$

respectively.

Finally, because in incompressible creeping-flow problems the nondimensional dynamic pressure gradient must be of order unity,²¹ we choose a viscous dynamic pressure scale,

$$\Pi' = \frac{\eta U}{L_v}. \tag{1.35}$$

A practical solution of the above equations, and hence of ferrofluid flow problems in the creeping translational and spin-flow limits, will require judicious assumptions of the relative magnitudes of the coefficients in (1.33) and (1.34), as well as in (1.31).

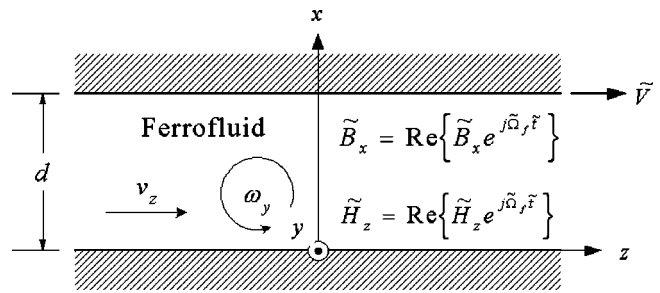


FIG. 1. Combined plane-Poiseuille and Couette flows of a ferrofluid subjected to time-varying magnetic fields along and transverse to the duct axis.

II. REGULAR PERTURBATION SOLUTION OF THE MAGNETIZATION EQUATION AND RESULTING MAGNETIC COUPLE

We apply the scaled magnetization equation, (1.31), to a planar ferrofluid layer confined between rigid walls of width d , as shown in Fig. 1. The imposed axial magnetic field H_z and transverse magnetic flux density B_x are spatially uniform and vary sinusoidally with time at radian frequency Ω_f . Because the fields are uniform with y and z coordinates, field components can only vary with the x coordinate. Gauss' law for the magnetic flux density and Ampère's law for the magnetic field intensity with zero current density then require the imposed fields to be spatially uniform, i.e., independent of x , but the resulting magnetization causes x dependent B_z and H_x components. The scaled magnetic field and flux density are thus of the form

$$\tilde{\mathbf{H}} = \text{Re}\{[\tilde{H}_x(x)\mathbf{i}_x + \tilde{H}_z\mathbf{i}_z]e^{j\tilde{\Omega}_f \tilde{t}}\}, \tag{2.1}$$

$$\tilde{\mathbf{B}} = \text{Re}\{[\tilde{B}_x\mathbf{i}_x + \tilde{B}_z(x)\mathbf{i}_z]e^{j\tilde{\Omega}_f \tilde{t}}\}, \tag{2.2}$$

where the time and field frequency have been scaled with respect to the ferrofluid relaxation time ($\tilde{\Omega}_f \equiv \tau \Omega_f$ and $\tilde{t} = t/\tau$), and the magnetic field and flux density have been normalized with respect to H and $\mu_0 H$, respectively, with H the magnitude of the total applied magnetic field in the absence of ferrofluid $\{H = |(B_x/\mu_0)\mathbf{i}_x + H_z\mathbf{i}_z| = [(B_x/\mu_0)^2 + H_z^2]^{1/2}\}$. Here we note that, in general, \tilde{B}_x , \tilde{H}_z , $\tilde{B}_z(\tilde{x})$, and $\tilde{H}_x(\tilde{x})$ are complex amplitudes, with the last two being functions of spatial position. The resulting magnetization field, force, and torque for this system have been obtained previously.⁷⁻⁹ Here we repeat this analysis, showing that the "small spin-velocity" approximation used in previous analyses⁷⁻⁹ is equivalent to a regular perturbation solution of the magnetization equation truncated after the first-order term.

A. Magnetization solution in the linear magnetization limit

Here we determine the magnetization and resultant body-force and body-couple when the equilibrium magnetization \mathbf{M}_{eq} in (1.4) is given by (1.12). Under conditions of fully developed, incompressible flow, the convective term in

the magnetization equation, (1.4), vanishes identically ($\mathbf{v} \cdot \nabla \mathbf{M} = \mathbf{0}$ and $\nabla \cdot \mathbf{v} = 0$ for the system of Fig. 1), as $\partial/\partial z$ of any quantity is taken to be zero in this fully developed flow, except for $\partial p'/\partial z$ which is taken to be a constant. Defining the perturbation parameter $\epsilon \equiv \tau\Omega$ as the product of the characteristic scale of the spin field, Ω , and the magnetization relaxation time scale of the ferrofluid, τ , and using $M \sim H$ as the scale for the magnetization vector, the magnetization equation, (1.18), becomes

$$\frac{\partial \tilde{\mathbf{M}}}{\partial \tilde{t}} = \epsilon \tilde{\boldsymbol{\omega}} \times \tilde{\mathbf{M}} - (\tilde{\mathbf{M}} - \chi_0 \tilde{\mathbf{H}}). \tag{2.3}$$

We seek a solution where the magnetization can be expressed as a power series expansion of the small parameter ϵ ,

$$\tilde{\mathbf{M}} = \sum_{n=0}^{\infty} \epsilon^n \tilde{\mathbf{M}}_n, \tag{2.4}$$

where the n th-order term of this regular perturbation expansion is assumed to have the same time dependence as the magnetic field (2.1) and magnetic flux density (2.2),

$$\tilde{\mathbf{M}}_n = \text{Re}\{[\tilde{M}_{n,x}(\tilde{x})\mathbf{i}_x + \tilde{M}_{n,z}(\tilde{x})\mathbf{i}_z]e^{j\tilde{\Omega}_f \tilde{t}}\}. \tag{2.5}$$

Prior work³³ in the cylindrical spin-up flow problem analogous to our parallel plate geometry has neglected the spin-reorientation term in the magnetization equation, as quantified by the first term on the right-hand side of (2.3). This is consistent with the truncation of the regular perturbation expansion at the first term of the series (zeroth order in ϵ). This so-called spin-diffusion theory analysis has been subsequently shown to predict spin-up flows which are orders of magnitude smaller than those observed experimentally.^{34,41} Alternative explanations for the observed spin-up flows, including surface-excess magnetic effects can be found in Rosensweig *et al.*³⁴ and Kaloni.³⁵

However, we note that other analyses⁷⁻⁹ have shown that keeping the effect of the spin-magnetization coupling, embodied by the $\boldsymbol{\omega} \times \mathbf{M}$ term in (2.3), can introduce novel flow behavior. That this is the case is further shown in our contribution, where the effect of spin-magnetization coupling is included by considering the first two terms of the regular perturbation expansion, ultimately resulting in a spin dependent portion of the body-torque density.

We also note that other analyses^{14,34,35} of the cylindrical spin-up flow of ferrofluid in the presence of a rotating magnetic field have assumed that the magnetization field \mathbf{M} is spatially uniform and found that spin velocity $\boldsymbol{\omega}$ is spatially dependent. However, in that case, as can be seen from the Appendix B solutions of Rosensweig *et al.*,³⁴ the magnetization field \mathbf{M} is also required to be spatially dependent. Hence these analyses^{14,34,35} lack self-consistency in their consideration of magnetization relaxation, a problem we avoid in our contribution by adopting the regular perturbation expansion scheme presented in this section.

1. Zeroth-order solutions

The zeroth-order problem is independent of the spin velocity and is given by

$$\frac{\partial \tilde{M}_{0,x}}{\partial \tilde{t}} = -(\tilde{M}_{0,x} - \chi_0 \tilde{H}_x), \tag{2.6a}$$

$$\frac{\partial \tilde{M}_{0,z}}{\partial \tilde{t}} = -(\tilde{M}_{0,z} - \chi_0 \tilde{H}_z). \tag{2.6b}$$

Upon substitution of the assumed form of the n th-order magnetization term, (2.5), into the zeroth-order magnetization equation we obtain

$$j\tilde{\Omega}_f \tilde{M}_{0,x} = -\tilde{M}_{0,x} + \chi_0 \tilde{H}_x, \tag{2.7a}$$

$$j\tilde{\Omega}_f \tilde{M}_{0,z} = -\tilde{M}_{0,z} + \chi_0 \tilde{H}_z. \tag{2.7b}$$

The x -directed magnetic field is related to the applied magnetic flux density field \mathbf{B} by

$$\tilde{H}_x = \tilde{B}_x - \tilde{M}_{0,x}. \tag{2.8}$$

The solution for the zeroth-order magnetization field is then

$$\tilde{M}_{0,x} = \frac{\chi_0}{(1 + \chi_0 + j\tilde{\Omega}_f)} \tilde{B}_x, \tag{2.9a}$$

$$\tilde{M}_{0,z} = \frac{\chi_0}{(1 + j\tilde{\Omega}_f)} \tilde{H}_z. \tag{2.9b}$$

2. nth-order solutions

The equations to solve for order $n \geq 1$ in ϵ are

$$\frac{\partial \tilde{M}_{n,x}}{\partial \tilde{t}} = \tilde{\omega}_y \tilde{M}_{n-1,z} - (1 + \chi_0) \tilde{M}_{n,x}, \tag{2.10a}$$

$$\frac{\partial \tilde{M}_{n,z}}{\partial \tilde{t}} = -\tilde{\omega}_y \tilde{M}_{n-1,x} - \tilde{M}_{n,z}. \tag{2.10b}$$

Note that we have not made any assumptions regarding the direction of the spin field at this stage. Components of the spin in the x and z directions do not appear here as we have assumed that $M_y = 0$. This reduces to the following system of linear algebraic equations:

$$j\tilde{\Omega}_f \tilde{M}_{n,x} = \tilde{\omega}_y \tilde{M}_{n-1,z} - (1 + \chi_0) \tilde{M}_{n,x}, \tag{2.11a}$$

$$j\tilde{\Omega}_f \tilde{M}_{n,z} = -\tilde{\omega}_y \tilde{M}_{n-1,x} - \tilde{M}_{n,z}. \tag{2.11b}$$

The recursive solution is simply

$$\tilde{M}_{n,x} = \tilde{\omega}_y \left(\frac{1}{1 + \chi_0 + j\tilde{\Omega}_f} \right) \tilde{M}_{n-1,z}, \tag{2.12a}$$

$$\tilde{M}_{n,z} = -\tilde{\omega}_y \left(\frac{1}{1 + j\tilde{\Omega}_f} \right) \tilde{M}_{n-1,x}. \tag{2.12b}$$

The n th-order magnetization (including order zero) for this set of ordinary difference equations, based on the applied fields is then

$$\tilde{M}_{n,x} = \begin{cases} (-1)^{(n-1)/2} \tilde{\omega}_y^n \left(\frac{1}{1+j\tilde{\Omega}_f} \right)^{(n+1)/2} \left(\frac{1}{1+\chi_0+j\tilde{\Omega}_f} \right)^{(n+1)/2} \chi_0 \tilde{H}_z, & n \text{ odd,} \\ (-1)^{n/2} \tilde{\omega}_y^n \left(\frac{1}{1+j\tilde{\Omega}_f} \right)^{n/2} \left(\frac{1}{1+\chi_0+j\tilde{\Omega}_f} \right)^{n/2+1} \chi_0 \tilde{B}_x, & n \text{ even,} \end{cases} \quad (2.13a)$$

$$\tilde{M}_{n,z} = \begin{cases} (-1)^{(n+1)/2} \tilde{\omega}_y^n \left(\frac{1}{1+j\tilde{\Omega}_f} \right)^{(n+1)/2} \left(\frac{1}{1+\chi_0+j\tilde{\Omega}_f} \right)^{(n+1)/2} \chi_0 \tilde{B}_x, & n \text{ odd,} \\ (-1)^{n/2} \tilde{\omega}_y^n \left(\frac{1}{1+j\tilde{\Omega}_f} \right)^{n/2+1} \left(\frac{1}{1+\chi_0+j\tilde{\Omega}_f} \right)^{n/2} \chi_0 \tilde{H}_z, & n \text{ even.} \end{cases} \quad (2.13b)$$

Using (2.13a) and (2.13b) we obtain for the first-order term in the regular perturbation expansion,

$$\tilde{M}_{1,x} = \tilde{\omega}_y \frac{\chi_0 \tilde{H}_z}{(1+j\tilde{\Omega}_f)(1+\chi_0+j\tilde{\Omega}_f)}, \quad (2.14a)$$

$$\tilde{M}_{1,z} = -\tilde{\omega}_y \frac{\chi_0 \tilde{B}_x}{(1+j\tilde{\Omega}_f)(1+\chi_0+j\tilde{\Omega}_f)}. \quad (2.14b)$$

The solution for the magnetization field, to first order in the small parameter $\epsilon = \Omega \tau$ is then

$$\tilde{\mathbf{M}} = \text{Re}\{[\tilde{M}_x \mathbf{i}_x + \tilde{M}_z \mathbf{i}_z] e^{j\tilde{\Omega}_f t}\}, \quad (2.15a)$$

$$\tilde{M}_x = \chi_0 \frac{(1+j\tilde{\Omega}_f)\tilde{B}_x + \epsilon \tilde{\omega}_y \tilde{H}_z}{(1+j\tilde{\Omega}_f)(1+\chi_0+j\tilde{\Omega}_f)} + O(\epsilon^2), \quad (2.15b)$$

$$\tilde{M}_z = \chi_0 \frac{(1+\chi_0+j\tilde{\Omega}_f)\tilde{H}_z - \epsilon \tilde{\omega}_y \tilde{B}_x}{(1+j\tilde{\Omega}_f)(1+\chi_0+j\tilde{\Omega}_f)} + O(\epsilon^2). \quad (2.15c)$$

These results agree with a Taylor series expansion with respect to the spin-velocity term in the magnetization results of previous analyses.⁷⁻⁹ Higher-order terms of the perturbation expansion for the magnetization vector can be easily obtained using (2.13).

B. *n*th-order time-averaged body-force density

The external body-force density \mathbf{f} on an incompressible ferrofluid is given by Eq. (1.8). Here we assume the gravitational field is constant throughout the system, as is the mass density ρ , hence the gravitational force is absorbed into the dynamic pressure as in (1.19). The remaining magnetic force \mathbf{f}^M is then

$$\mathbf{f}^M = \mu_0 \left(M_x \frac{dH_x}{dx} \mathbf{i}_x + M_x \frac{dH_z}{dx} \mathbf{i}_z \right). \quad (2.16)$$

However, as discussed above, H_z is independent of x , therefore the z -directed component of the force is zero identically. The x -directed component can be simplified by using the relation

$$H_x = \frac{1}{\mu_0} B_x - M_x. \quad (2.17)$$

Then we obtain for the x -component of the magnetic force,

$$f_x^M = -\frac{d}{dx} \left(\frac{\mu_0}{2} M_x^2 \right). \quad (2.18)$$

The time-averaged magnetic force is then

$$\langle \mathbf{f}^M \rangle = -\frac{d}{dx} \frac{\mu_0}{2} \langle M_x^2 \rangle \mathbf{i}_x. \quad (2.19)$$

Because the time-averaged magnetic body-force can be expressed as the gradient of a scalar function, a new dynamic pressure p'' may be defined⁷⁻⁹ as

$$p'' = p - \rho(\mathbf{g} \cdot \mathbf{r}) + \frac{\mu_0}{2} \langle M_x^2 \rangle. \quad (2.20)$$

Such a definition can be obtained by considering the x -component of the time-averaged linear momentum equation. However, we note that because magnetization is not a function of z , this additional term does not affect the z -directed flows obtained below. The dynamic pressure p' referred to in what follows is that defined in Eq. (1.19).

C. *n*th-order time-averaged body-couple density

The body-couple density \mathbf{l} due to a quasistatic magnetic field on a ferrofluid suspension is given by (1.9). Owing to the time dependent fields of the form given in (2.1)–(2.2), the body-couple will also be a function of time. However, in this analysis we are only interested in the time-averaged behavior of the ferrofluid suspension as we assume that fluid inertia and viscosity prevent the fluid from significantly responding to the 2nd harmonic magnetic force and torque. The resulting time-averaged body-couple density is solely in the y -direction and is given by⁷⁻⁹

$$\langle \tilde{l}_y \rangle = \frac{1}{2} \text{Re}\{ \tilde{M}_z \tilde{B}_x^* - \tilde{M}_x^* (\tilde{H}_z + \tilde{M}_z) \}, \quad (2.21)$$

with the superscript $*$ denoting the complex conjugate of a complex amplitude term. In writing (2.21), we have assumed that the spin velocity appearing in (2.13) is independent of time, a relatively good assumption when one considers situations where the characteristic time scale for changes in the magnetic quantities Ω_f^{-1} is small compared to the inertial/viscous time scale $\tau_{iv} \sim L_v^2 \rho / \eta$. In any case, the difference is assumed here to be very small.

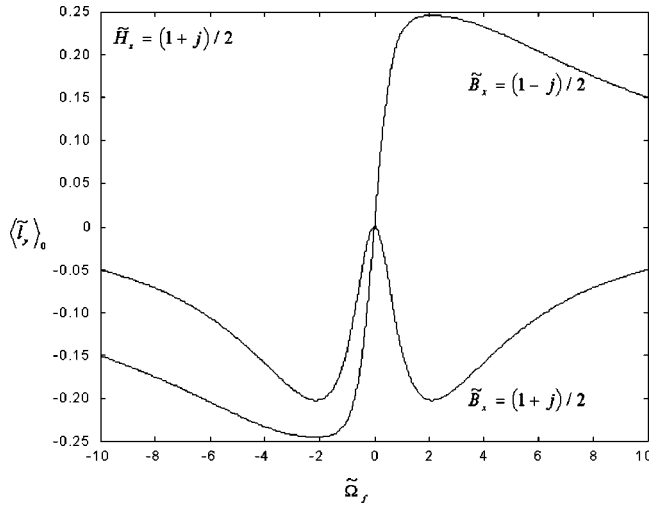


FIG. 2. Zeroth-order body-couple term $\langle \tilde{T}_y \rangle_0$ vs $\tilde{\Omega}_f$ for $\chi_0=3.5$, $\tilde{H}_z=(1+j)/2$, and $\tilde{B}_x=(1\pm j)/2$.

Because it depends quadratically on the magnetization field, the body-couple density can also be written as an expansion in terms of the perturbation parameter ϵ ,

$$\langle \tilde{T}_y \rangle = \sum_{n=0}^{\infty} \epsilon^n \langle \tilde{T}_y \rangle_n, \tag{2.22}$$

with the n th-order term given by

$$\langle \tilde{T}_y \rangle_n = \frac{1}{2} \text{Re} \left\{ \tilde{M}_{n,z} \tilde{B}_x^* - \tilde{M}_{n,x}^* \tilde{H}_z - \sum_{i=0}^n \tilde{M}_{n-i,x}^* \tilde{M}_{i,z} \right\}. \tag{2.23}$$

We are particularly interested in the properties of the zeroth and first-order terms of this perturbation expansion.

1. Properties of the zeroth-order body-couple term $\langle \tilde{T}_y \rangle_0$

Using (2.23), we obtain for the zeroth-order term,

$$\begin{aligned} \langle \tilde{T}_y \rangle_0 &= \frac{1}{2} \text{Re} \{ \tilde{M}_{0,z} \tilde{B}_x^* - \tilde{M}_{0,x}^* \tilde{H}_z - \tilde{M}_{0,x}^* \tilde{M}_{0,z} \} \\ &= -\chi_0 \frac{\text{Re} \{ [\chi_0 \tilde{\Omega}_f^2 + j \tilde{\Omega}_f (\tilde{\Omega}_f^2 + 1 + \chi_0)] [\tilde{B}_x^* \tilde{H}_z] \}}{(1 + \chi_0 + \tilde{\Omega}_f^2)^2 + \chi_0^2 \tilde{\Omega}_f^2}, \end{aligned} \tag{2.24}$$

in agreement with previous results,⁷⁻⁹ where the symbol T_y was used to denote the body-couple density. Here we reserve the symbol \mathbf{T} for the Cauchy stress and its components and use l_y for the body-couple density instead. Figure 2 shows representative plots of the zeroth-order body-couple term and it's variation with the scaled field frequency $\tilde{\Omega}_f$. Note that $\langle \tilde{T}_y \rangle_0 = 0$ if either \tilde{B}_x or \tilde{H}_z are zero.

As shown in Fig. 2, the zeroth-order body-couple term typically has extreme values with respect to the field frequency. The criterion for extrema with respect to the field frequency is

$$\frac{\partial}{\partial \tilde{\Omega}_f} \langle \tilde{T}_y \rangle_0 = 0. \tag{2.25}$$

It is a simple exercise to verify that this criterion is met when

$$\tilde{\Omega}_f = \pm \sqrt{1 + \chi_0}, \tag{2.26}$$

and when

$$\begin{aligned} 2\chi_0 \tilde{\Omega}_f (\chi_0 + 1 + \tilde{\Omega}_f^2) \text{Re} \{ [\tilde{B}_x^* \tilde{H}_z] \} - (\tilde{\Omega}_f^2 + \chi_0 \tilde{\Omega}_f + \chi_0 + 1) \\ \times (\tilde{\Omega}_f^2 - \chi_0 \tilde{\Omega}_f + \chi_0 + 1) \text{Im} \{ [\tilde{B}_x^* \tilde{H}_z] \} = 0. \end{aligned} \tag{2.27}$$

When \tilde{B}_x and \tilde{H}_z are in phase such that the term $[\tilde{B}_x^* \tilde{H}_z]$ is purely real we have three distinct real roots of (2.27), given by (2.26) and

$$\tilde{\Omega}_f = 0. \tag{2.28}$$

When \tilde{B}_x and \tilde{H}_z are 90° out of phase such that the term $[\tilde{B}_x^* \tilde{H}_z]$ is purely imaginary we have two distinct real roots (for $0 < \chi_0 < 2 + 2\sqrt{2}$, a generally good assumption) given by (2.26). There are four additional real roots to (2.25) when $\chi_0 > 2 + 2\sqrt{2}$, given by

$$\tilde{\Omega}_f = \frac{\pm \chi_0 \pm [(\chi_0 - 2 - 2\sqrt{2})(\chi_0 - 2 + 2\sqrt{2})]^{1/2}}{2}. \tag{2.29}$$

Cases when the $[\tilde{B}_x^* \tilde{H}_z]$ term is complex are more involved but will always possess the roots given in (2.26).

From (2.24), the zeroth-order body-couple is always zero when the excitation frequency is zero. At the roots given by (2.26) we have that the zeroth-order body-couple is

$$\begin{aligned} \langle \tilde{T}_y \rangle_0 |_{\tilde{\Omega}_f = \pm \sqrt{1 + \chi_0}} &= -\frac{\chi_0^2 \text{Re} \{ [\tilde{B}_x^* \tilde{H}_z] \}}{(2 + \chi_0)^2} \\ &\pm \frac{2\chi_0 \sqrt{1 + \chi_0} \text{Im} \{ [\tilde{B}_x^* \tilde{H}_z] \}}{(2 + \chi_0)^2}. \end{aligned} \tag{2.30}$$

For purely real and positive $[\tilde{B}_x^* \tilde{H}_z]$ this corresponds to two $-y$ -directed extrema. For purely imaginary and positive $[\tilde{B}_x^* \tilde{H}_z]$ this corresponds to a $+y$ -directed extremum at $\tilde{\Omega}_f = \sqrt{1 + \chi_0}$ and a $-y$ -directed extremum at $\tilde{\Omega}_f = -\sqrt{1 + \chi_0}$. Reversing the sign of the $[\tilde{B}_x^* \tilde{H}_z]$ term merely reverses the direction of these extrema in the zeroth-order body-couple.

2. Properties of the first-order body-couple term $\langle \tilde{T}_y \rangle_1$

Using (2.23), the first-order term is

$$\begin{aligned} \langle \tilde{T}_y \rangle_1 &= \frac{1}{2} \text{Re} \{ \tilde{M}_{1,z} \tilde{B}_x^* - \tilde{M}_{1,x}^* \tilde{H}_z - \tilde{M}_{1,x}^* \tilde{M}_{0,z} - \tilde{M}_{0,x}^* \tilde{M}_{1,z} \}, \\ &= \chi_0 \tilde{\omega}_y \frac{1}{2} \frac{(\tilde{\Omega}_f^2 - 1) |\tilde{B}_x|^2 + (\tilde{\Omega}_f^2 - (1 + \chi_0)^2) |\tilde{H}_z|^2}{(1 + \chi_0 + \tilde{\Omega}_f^2)^2 + \chi_0^2 \tilde{\Omega}_f^2}, \end{aligned} \tag{2.31}$$

in agreement with previous work.⁷⁻⁹ For consistency with previous work,⁷⁻⁹ and to simplify the form of the equations to follow in the next section, we define the parameter α ,

$$\alpha = \langle \tilde{T}_y \rangle_1 / \tilde{\omega}_y = \chi_0 \frac{1}{2} \frac{(\tilde{\Omega}_f^2 - 1)|\tilde{B}_x|^2 + (\tilde{\Omega}_f^2 - (1 + \chi_0)^2)|\tilde{H}_z|^2}{(1 + \chi_0 + \tilde{\Omega}_f^2) + \chi_0^2 \tilde{\Omega}_f^2}. \quad (2.32)$$

Figure 3 is a representative plot of α and its variation with the field frequency.

As with the zeroth-order body-couple term, we are interested in finding extreme values of the spin-independent portion of the first-order body-couple term with respect to the field frequency, given by the criterion

$$\frac{\partial}{\partial \tilde{\Omega}_f} \alpha = 0. \quad (2.33)$$

As can be verified, this is always satisfied when the field frequency is zero, $\tilde{\Omega}_f = 0$, which corresponds to a minimum in α :

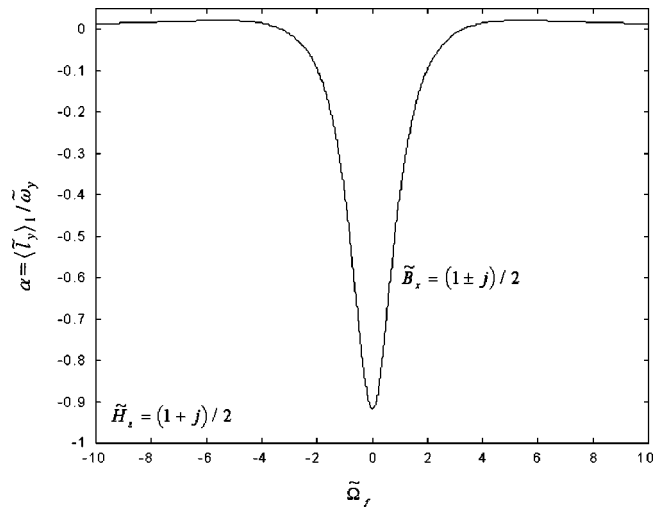


FIG. 3. First-order body-couple term $\alpha(\langle \tilde{T}_y \rangle_1 / \tilde{\omega}_y)$ vs $\tilde{\Omega}_f$ for $\chi_0 = 3.5$, $\tilde{H}_z = (1 + j)/2$, and $\tilde{B}_x = (1 \pm j)/2$.

$$\alpha|_{\tilde{\Omega}_f=0} = -\frac{1}{2} \chi_0 \frac{|\tilde{B}_x|^2 + (1 + \chi_0)^2 |\tilde{H}_z|^2}{(1 + \chi_0)^2}. \quad (2.34)$$

The other real roots of the extremum criterion in (2.33) are

$$\tilde{\Omega}_f = \pm \left[\frac{|\tilde{B}_x|^2 + |\tilde{H}_z|^2 (1 + \chi_0)^2}{|\tilde{B}_x|^2 + |\tilde{H}_z|^2} + \frac{\sqrt{(2|\tilde{B}_x|^2 + |\tilde{H}_z|^2 (1 + (1 + \chi_0)^2)) (|\tilde{B}_x|^2 (1 + (1 + \chi_0)^2) + 2|\tilde{H}_z|^2 (1 + \chi_0)^2)}}{|\tilde{B}_x|^2 + |\tilde{H}_z|^2} \right]^{1/2}. \quad (2.35)$$

Note that, in contrast with the zeroth-order body-couple term, the first-order body-couple term always has these three extreme values (one $-y$ -directed and two $+y$ -directed extrema).

As will be seen in what follows, the maximum value of α will be important in determining what flow regimes are possible for the configuration being analyzed in this paper. This maximum value is obtained for a given set $\{\chi_0, \tilde{B}_x, \tilde{H}_z\}$ using (2.35) in (2.32). As an example, for $|\tilde{H}_z|^2 = 0$ extreme values occur for field frequencies given by

$$\tilde{\Omega}_f = \pm [1 + \sqrt{2 + 2(1 + \chi_0)^2}]^{1/2}, \quad (2.36)$$

which correspond to an α value of³⁶

$$\alpha|_{\tilde{H}_z=0}^{\max} = \frac{1}{2} \frac{\chi_0}{3 + (1 + \chi_0)^2 + 2\sqrt{2 + 2(1 + \chi_0)^2}}. \quad (2.37)$$

Other situations can be similarly obtained, but note that in general the maximum values of α will be less than unity. For a representative value of the magnetic susceptibility $\chi_0 = 3.5$ (see Sec. I A 3) we have that $\alpha|_{\tilde{H}_z=0}^{\max} = 4.8 \times 10^{-2}$. The parameter α also possesses extrema with respect to the mag-

netic susceptibility χ_0 , for example, starting from (2.37) an extremum is found for $\chi_0 = 2.73205$ with $\alpha|_{\tilde{H}_z=0}^{\max} = 4.9 \times 10^{-2}$.

As we have mentioned before, we are interested in the effect of keeping the first two terms in the body-couple perturbation expansion. These two terms correspond to the small spin-velocity body-couple density used in previous analyses,⁷⁻⁹

$$\langle \tilde{T}_y \rangle = \tilde{T}_0 + \epsilon \alpha \tilde{\omega}_y, \quad (2.38)$$

with \tilde{T}_0 given by $\langle \tilde{T}_y \rangle_0$ and α as defined in (2.32). From here on, we will refer to \tilde{T}_0 ($\equiv \langle \tilde{T}_y \rangle_0$) as the zeroth-order body-couple term and α ($\equiv \langle \tilde{T}_y \rangle_1 / \omega_y$) as the first-order body-couple term.

With the preceding analysis it is easy to see that the “small spin-velocity limit” for the body-couple density used in previous work⁷⁻⁹ is equivalent to truncation after the first-order term of a regular perturbation expansion of the magnetization equation, with the small parameter ϵ . Because in practical applications ϵ will indeed be a small parameter, this linear body-couple density expression should be widely applicable.

III. TRANSLATIONAL AND SPIN-VELOCITY SOLUTIONS

The analysis in this section is for the asymptotic limit of fully developed, uniaxial (along the z -axis in Fig. 1) flow of an incompressible ferrofluid between two parallel plates. Based on the imposed boundary conditions and symmetries of the flow geometry, the time-average flow fields are expected to be of the form

$$\mathbf{v}(\mathbf{x}) = v_z(x)\mathbf{i}_z, \tag{3.1a}$$

$$\boldsymbol{\omega}(\mathbf{x}) = \omega_y(x)\mathbf{i}_y. \tag{3.1b}$$

Note that the condition $\nabla \cdot \boldsymbol{\omega} = 0$ is satisfied exactly by this assumed flow situation. This is because the x -component of the spin is required to be zero. A nonzero x -component in the spin velocity would result in nonzero x - and y -components for the translational velocity, thereby contradicting the assumption of uniaxial flow. This is analogous to the cylindrical symmetry argument used in the analysis of ferrofluid entrainment in a rotating magnetic field.^{14,33-35}

A solution for this creeping-flow problem in the limit of negligible spin diffusion ($\eta' \rightarrow 0$) has been given elsewhere.⁷⁻⁹ Here we extend the analysis to include the effects of spin diffusion, allow for relative movement between the parallel plates, and examine the effects of boundary conditions on spin velocity.

The time-averaged momentum equations for the system, scaled as discussed in Sec. I B 4, are given by (1.33) and (1.34). Because we are interested in a single region flow, we assume the characteristic length scales for variations in translational and spin-velocities are the same and equal to the characteristic macroscopic linear dimension of the problem, the gap width d ,

$$L_v = L_\omega = d. \tag{3.2}$$

Furthermore, to simplify the form of the equations that follow, we set

$$\frac{\Omega d}{U} = 1, \tag{3.3}$$

which is equivalent to scaling the spin field with the vorticity field.

Considering the assumed form of the flow field (3.1), only the z -component of the linear momentum equation and the y -component of the internal angular momentum equation are of concern. Note that the time-averaged x -component of the same equation does not provide additional information, besides the definition of second dynamic pressure, p'' , independent to x , as discussed in Sec. II B. In rectangular coordinates, the time-averaged z -component of the linear momentum equation in the creeping-flow limit, (1.33), reduces to

$$\frac{\eta_e}{\eta} \frac{d^2 \tilde{v}_z}{d\tilde{x}^2} + 2 \frac{\zeta}{\eta} \frac{d\tilde{\omega}_y}{d\tilde{x}} - \frac{\partial p''}{\partial \tilde{z}} = 0, \tag{3.4}$$

where $\eta_e = \eta + \zeta$ and we have used the fact that the time-averaged z -directed magnetic body-force is zero.⁷⁻⁹

The corresponding time-averaged y -component of the internal angular momentum equation in the creeping-flow limit, (1.34), reduces to

$$\left(\frac{\eta'}{\zeta d^2} \right) \frac{d^2 \tilde{\omega}_y}{d\tilde{x}^2} - 2 \frac{d\tilde{v}_z}{d\tilde{x}} - 4 \tilde{\omega}_y + \left(\frac{\mu_0 H^2}{\zeta \Omega} \right) \langle \tilde{T}_y \rangle = 0. \tag{3.5}$$

Next, we introduce the assumed linear form of the body couple density, $\langle \tilde{T}_y \rangle$, (2.38), into the internal angular momentum equation, to obtain

$$\left(\frac{\eta'}{\zeta d^2} \right) \frac{d^2 \tilde{\omega}_y}{d\tilde{x}^2} - 2 \frac{d\tilde{v}_z}{d\tilde{x}} + \left[\left(\frac{\mu_0 H^2}{\zeta \Omega} \right) \epsilon \alpha - 4 \right] \tilde{\omega}_y + \left(\frac{\mu_0 H^2}{\zeta \Omega} \right) \tilde{T}_0 = 0. \tag{3.6}$$

The solutions of (3.4) and (3.6) and their interpretation in various limiting conditions are the focus of this section. In these solutions we can identify three important dimensionless parameters. The first is the ratio of vortex and shear viscosities, ζ/η , which, according to Brenner,¹² is proportional to the volume fraction ϕ of magnetic particles in the suspension,³⁷

$$\frac{\zeta}{\eta} = \frac{3}{2} \phi. \tag{3.7}$$

The second dimensionless parameter is the ratio of spin viscosity to vortex viscosity divided by the macroscopic length scale squared, $\eta' / (\zeta d^2)$. This ratio is in fact a ratio of macroscopic and intrinsic length scales. This is easily seen if one considers that the spin-viscosity is expected to be a function of the shear viscosity of the ferrofluid, its volume fraction, and a characteristic length scale L_p squared, obtaining

$$\frac{\eta'}{\zeta d^2} \propto \frac{L_p^2}{d^2}. \tag{3.8}$$

This expected functionality, coupled with the *assumption* that the intrinsic length scale L_p is of the order of the particle diameter is the usual motivation for neglecting the first term of Eq. (3.6). However, even in cases where this parameter is indeed negligibly small, the combined effects of spin diffusion and spin/vorticity coupling will result in the formation of boundary layers near walls and interfaces. These boundary layers could have a profound effect on shear stresses at these walls or interfaces, thereby giving their consideration signal importance in any experimental determination of ferrofluid properties through these measurements.

The third and final parameter is the ratio of ‘‘pumping’’ of intrinsic angular momentum through the body-couple mechanism to interconversion of external/internal angular momentum through the vorticity/spin coupling in the structured fluid,

$$\frac{\mu_0 H^2}{\zeta \Omega}. \tag{3.9}$$

Because we are interested in keeping the effect of the first-order body-couple term on the internal angular momentum equation (3.6), we require

$$\left(\frac{\mu_0 H^2}{\zeta \Omega}\right) \epsilon = \frac{\mu_0 H^2 \tau}{\zeta} \sim 1. \tag{3.10}$$

This constitutes a requirement on the magnetic field magnitude for significant magnetization/spin-velocity interaction. For a typical ferrofluid ($\zeta/\eta \sim 0.15$, $\phi = 0.1$, $\eta \sim 0.03 \text{ Nsm}^{-2}$, $\tau \sim 10^{-5} \text{ s}$) this will require $\mu_0 H \sim 230 \text{ G}$. This value of the required magnetic field somewhat exceeds the estimated threshold value of $\mu_0 H \sim 52 \text{ G}$ valid for the linear magnetization limit (see Sec. I A 3). This indicates that (1.12) might not be an accurate model for \mathbf{M}_{eq} when applied to magnetic fields that exceed 52 G.

It could be inferred that this requirement on the magnetic field magnitude introduces a scaling problem in the internal angular momentum, (3.6), because the coefficient of the \tilde{T}_0 term will be very large, however, this is not necessarily the case as the magnitude of \tilde{T}_0 may be made as small as required independently of the magnitude of α .³⁸

A. Zero-spin-viscosity solution

First we reproduce the analytical solution for zero-spin-viscosity flow given in previous work,⁷⁻⁹ extending it to allow for relative movement between the plates. The relevant equations are (3.4) and (3.6) with the parameter $\eta' / (\zeta d^2)$ set to zero. Because the second-order spatial derivative has been dropped from the internal angular momentum equation, we no longer require spatial boundary conditions for the spin field. The usual no-slip boundary condition is applied on the translational velocity field at the bounding walls,

$$\tilde{v}_z(0) = 0, \quad \tilde{v}_z(1) = \tilde{V}, \tag{3.11}$$

where $\tilde{V} (\equiv V/U)$ is the dimensionless velocity of the upper plate, made dimensionless with respect to the characteristic translational velocity U . Note that \tilde{V} is $O(1)$ or less, as the magnitude of the translational velocity field is likewise affected by the pressure gradient, through (1.35), and the spin/vorticity coupling mechanism assumed in (3.3).

The resulting translational velocity field is

$$\tilde{v}_z(\tilde{x}) = -\frac{\tilde{x}(1-\tilde{x})}{2\eta_m/\eta} \frac{\partial \tilde{p}'}{\partial \tilde{z}} + \tilde{V}\tilde{x}. \tag{3.12}$$

This equation is similar in form to the classical solution for flow of an unstructured Newtonian fluid under similar conditions.³⁹ This is partly the motivation for coining the term ‘‘magnetoviscosity’’ for the algebraically signed scalar η_m . This magnetoviscosity is given by the relation

$$\eta_m = \eta + \frac{\alpha \zeta}{\alpha - 4[(\mu_0 H^2 / \zeta \Omega) \epsilon]^{-1}}. \tag{3.13}$$

This result is equivalent to that given previously.⁷⁻⁹ The dependence of η_m with respect to α is shown graphically in Fig. 4. Notice that η_m is a discontinuous function of α , with the discontinuity occurring at

$$\alpha_d = 4 \left[\left(\frac{\mu_0 H^2}{\zeta \Omega} \right) \epsilon \right]^{-1}. \tag{3.14}$$

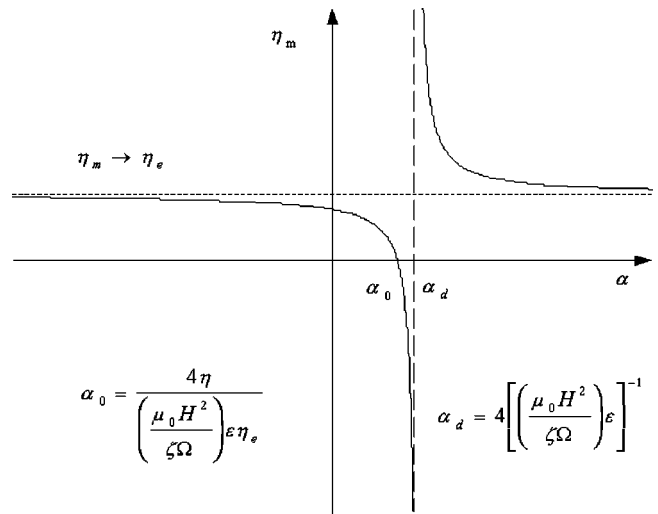


FIG. 4. Graph of Eq. (3.13), showing the major features of the dependence of η_m on α . As $\alpha \rightarrow \pm\infty$ we have $\eta_m \rightarrow \eta_e$. The value α_0 , corresponding to $\eta_m = 0$, is given by Eq. (3.16) and α_d , corresponding to a discontinuity in η_m , is given by Eq. (3.14).

Also notice that there is an asymptote for $\eta_m \rightarrow \eta_e$ as $\alpha \rightarrow \pm\infty$. Owing to our discussion on the bounds of α in Sec. II C 2, this is clearly impossible. Figure 5 shows representative curves of η_m vs $\tilde{\Omega}_f$. In this figure we show that the present model requires $(\mu_0 H^2 / \zeta \Omega) \epsilon \equiv (\mu_0 H^2 \tau / \zeta) \sim 70$, corresponding to a magnetic field of $\mu_0 H \sim 1900 \text{ G}$ (using $\eta = 0.03 \text{ Nm}^{-2}\text{s}$, $\zeta/\eta = 0.15$, and $\tau = 10^{-5}$) to achieve the so-called ‘‘negative viscosity’’ regime. This is in stark disagreement with the experimental evidence, where smaller magnetic fields have been found to produce the ‘‘negative viscosity’’ effect. This indicates that it is likely that magnetic body forces due to field gradients in the flow direction (or opposite to it) are responsible for the experimentally observed flows. Such body force effects do not arise in the uniform field configuration studied here, but in most practical realizations of magnetic field configurations it is difficult

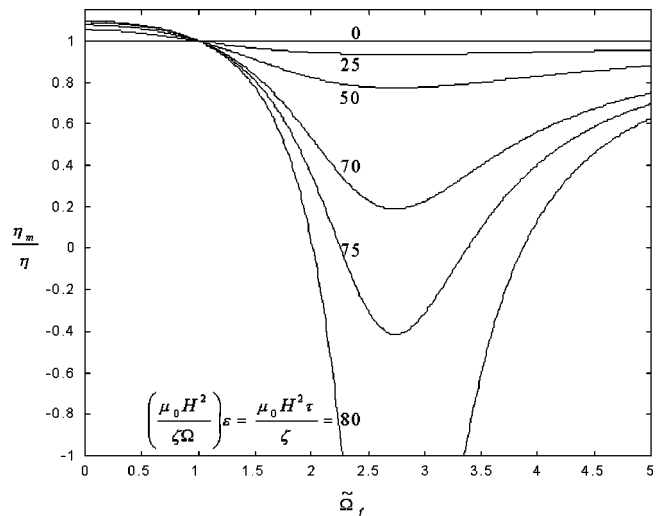


FIG. 5. Graph of η_m dependence on $\tilde{\Omega}_f$ for $\chi_0 = 3.5$, $\tilde{H}_z = 0$, and $\tilde{B}_x = 1$. Various values of $(\mu_0 H^2 / \zeta \Omega) \epsilon = \mu_0 H^2 \tau / \zeta$ are shown.

to have a perfectly uniform magnetic field and it is possible that in reported experiments small magnetic field nonuniformities have significant effects on the flow.

Solving (3.13) for α we obtain

$$\alpha = \frac{4(\eta - \eta_m)}{(\mu_0 H^2 / \zeta \Omega) \epsilon (\eta_e - \eta_m)}, \quad (3.15)$$

which will be used in the next section to rewrite the internal angular momentum equation in terms of the magnetoviscosity.

Because a sign change in η_m corresponds to a predicted flow reversal (in the limit $\eta' \rightarrow 0$), it is interesting to consider conditions for which this will occur. The value of α for which the effective viscosity is zero is

$$\alpha_0 = \frac{4\eta}{(\mu_0 H^2 / \zeta \Omega) \epsilon \eta_e}. \quad (3.16)$$

Using this and the fact that the maximum attainable first-order body torque yields $\alpha \sim 5 \times 10^{-2}$ we obtain that the required magnetic field magnitude for negative effective viscosities according to this model is $\mu_0 H \sim 1900$ G, in agreement with the approximate value provided above.

It is interesting to see what happens to the magnetoviscosity in the limit of small ϵ , when the product $(\mu_0 H^2 / \zeta \Omega) \epsilon$ is much less than unity. In that case we obtain for η_m ,

$$\eta_m \cong \eta - \frac{1}{4} \alpha \left(\frac{\mu_0 H^2}{\Omega} \right) \epsilon + O(\epsilon^2). \quad (3.17)$$

To order $O(\epsilon)$, the magnetoviscosity will be zero for

$$\alpha = \frac{4\eta}{\mu_0 H^2 \tau}. \quad (3.18)$$

With a representative value of $\mu_0 H \sim 230$ G, $\tau = 10^{-5}$ s, and $\eta = 0.03$ Nsm⁻², this requires $\alpha \sim 28$. Based on our discussion on the magnitude of α ($\sim 5 \times 10^{-2}$) in Sec. II C 2, such a large value will not be possible, showing that the assumption in (3.10) is necessary to obtain the desired flow-reversal behavior in this model.

Finally, using (3.13) to calculate the effective viscosity in the small magnetization limit (using $\mu_0 H \sim 52$ G) predicts that the maximum decrease obtainable is less than 0.01% ($\eta_m / \eta \sim 0.9999$). This further indicates that the linear magnetization assumption, (1.12), might not be a good model for these experiments and that considering the magnetic saturation limit may be necessary.

The solution for the spin-velocity field in the zero-spin-viscosity limit is

$$\tilde{\omega}_y(\tilde{x}) = \frac{(\eta_e - \eta_m)}{4\zeta} \left[\left(\frac{\mu_0 H^2}{\Omega \zeta} \right) \tilde{I}_0 - 2\tilde{V} + \frac{(1 - 2\tilde{x})}{\eta_m / \eta} \frac{\partial \tilde{p}'}{\partial \tilde{z}} \right]. \quad (3.19)$$

Because the difference between the spin-velocity and the vorticity is a measure of the system's departure from equilibrium¹¹ and is used in estimating mechanical energy dissipation in the flow,²⁰ we present the resulting vorticity ($\Omega = \nabla \times \mathbf{v}$) for the flow when spin-viscosity is neglected,

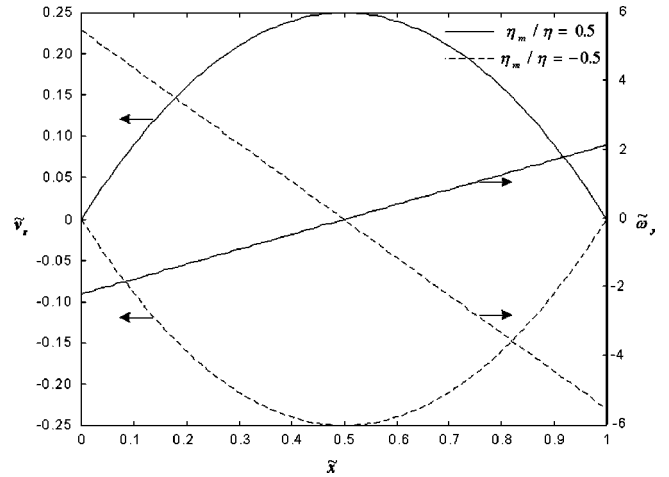


FIG. 6. Translational and spin-velocity profiles for the zero-spin-viscosity solution, Eqs. (3.12) and (3.19), with $\zeta/\eta = 0.15$, $\eta_m/\eta = \pm 0.5$, $\partial \tilde{p}' / \partial \tilde{z} = -1$, $\tilde{V} = 0$, and $(\mu_0 H^2 / \zeta \Omega) \tilde{I}_0 = 0$. Changing the value of this last parameter merely translates the spin-velocity curve along the abscissa.

$$\tilde{\Omega}_y(\tilde{x}) = - \frac{d\tilde{v}_z}{d\tilde{x}} = \frac{(1 - 2\tilde{x})}{2\eta_m / \eta} \frac{\partial \tilde{p}'}{\partial \tilde{z}} - \tilde{V}. \quad (3.20)$$

Figure 6 shows representative plots of the translational and spin-velocity for the case when the spin-viscosity is neglected in the internal angular momentum equation and $\tilde{V} = 0$. In this, as in all plots in this paper, we have taken $\partial \tilde{p}' / \partial \tilde{z} = -1$. Note that the slopes of the (linear) spin-velocity are not required to simply reverse sign when the algebraic sign of η_m reverses (the way the vorticity does), as seen from (3.19). The translational velocity profiles exhibit the classical parabolic shape, but with a discontinuity (infinite flow) when $\eta_m = 0$. Adding the effect of relative plate movement merely superposes a linear translational velocity profile and translates the spin-velocity profile along the abscissa accordingly.

Because the volumetric flow rate is the most easily measured flow property for ferrofluids, we provide the expected volumetric flow rate (per unit channel depth), scaled with respect to the translational velocity scale U and channel cross-section d of the channel [$\tilde{Q} = Q / (Ud)$],

$$\tilde{Q} = \int_0^1 \tilde{v}_z d\tilde{x} = - \frac{1}{12} \frac{\eta}{\eta_m} \frac{\partial \tilde{p}'}{\partial \tilde{z}}. \quad (3.21)$$

From (3.21) it is easy to see that neglecting the effect of spin-diffusion in the internal angular momentum equation results in a predicted flow rate which becomes infinite (as do the translational and spin-velocities) when the magnetic field dependent effective viscosity η_m becomes zero.

B. Nonzero-spin-viscosity solution (spin no-slip at boundaries)

Upon using (3.15) to express α in terms of η_m , the internal angular momentum, (3.6), becomes

$$\left(\frac{\eta'}{\zeta d^2}\right) \frac{d^2 \tilde{\omega}_y}{d\tilde{x}^2} - 2 \frac{d\tilde{v}_z}{d\tilde{x}} - \frac{4\zeta}{(\eta_e - \eta_m)} \tilde{\omega}_y + \left(\frac{\mu_0 H^2}{\zeta \Omega}\right) \tilde{l}_0 = 0. \tag{3.22}$$

This and (3.4) form a set of two coupled second-order ordinary differential equations. To solve them we take the derivative with respect to \tilde{x} of the internal angular momentum equation, (3.22), and substitute it into the linear momentum equation, (3.4), resulting in a third-order ordinary differential equation in the spin velocity $\tilde{\omega}_y$. The translational velocity is obtained in turn from the internal angular momentum equation, (3.22). The equations to solve for the spin and translational velocity are, respectively,

$$\frac{\eta_e}{\eta} \left(\frac{\eta'}{\zeta d^2}\right) \frac{d^3 \tilde{\omega}_y}{d\tilde{x}^3} - \frac{4\zeta \eta_m}{\eta(\eta_e - \eta_m)} \frac{d\tilde{\omega}_y}{d\tilde{x}} - 2 \frac{\partial \tilde{p}'}{\partial \tilde{z}} = 0, \tag{3.23}$$

and

$$\frac{d\tilde{v}_z}{d\tilde{x}} = \frac{1}{2} \left(\frac{\eta'}{\zeta d^2}\right) \frac{d^2 \tilde{\omega}_y}{d\tilde{x}^2} - \frac{2\zeta}{(\eta_e - \eta_m)} \tilde{\omega}_y + \frac{1}{2} \left(\frac{\mu_0 H^2}{\zeta \Omega}\right) \tilde{l}_0. \tag{3.24}$$

In this section we are interested in the solution to these equations when the spin-velocity vanishes at the container walls; hence the boundary conditions

$$\tilde{v}_z(0) = 0, \quad \tilde{v}_z(1) = \tilde{V}, \tag{3.25a}$$

$$\tilde{\omega}_y(0) = 0, \quad \tilde{\omega}_y(1) = 0. \tag{3.25b}$$

The resulting translational and spin-velocity profiles are

$$\begin{aligned} \tilde{v}_z(\tilde{x}) = & - \left[\frac{\tilde{x}(1-\tilde{x})\eta}{2\eta_m} + \frac{\eta(\eta_e - \eta_m)}{2\eta_e\eta_m} \frac{(1 + \cos \kappa)(1 - \cos \kappa\tilde{x}) - \sin \kappa \sin \kappa\tilde{x}}{\kappa \sin \kappa} \right] \frac{\partial \tilde{p}'}{\partial \tilde{z}} + \tilde{V}\tilde{x} \\ & + \left[\frac{(\eta_e - \eta_m)}{2\eta_e} \frac{(1 - \cos \kappa)(1 - 2\tilde{x} - \cos \kappa\tilde{x}) + \sin \kappa \sin \kappa\tilde{x}}{\kappa \sin \kappa - 2[(\eta_e - \eta_m)/\eta_e](1 - \cos \kappa)} \right] \left[\left(\frac{\mu_0 H^2}{\zeta \Omega}\right) \tilde{l}_0 - 2\tilde{V} \right], \end{aligned} \tag{3.26}$$

and

$$\begin{aligned} \tilde{\omega}_y(\tilde{x}) = & \frac{\eta(\eta_e - \eta_m)}{4\zeta\eta_m} \left[1 - 2\tilde{x} - \cos \kappa\tilde{x} + \frac{(1 + \cos \kappa)\sin \kappa\tilde{x}}{\sin \kappa} \right] \frac{\partial \tilde{p}'}{\partial \tilde{z}} + \left[\frac{(\eta_e - \eta_m)}{4\zeta} \frac{\kappa \sin \kappa(1 - \cos \kappa\tilde{x}) - (1 - \cos \kappa)\kappa \sin \kappa\tilde{x}}{\kappa \sin \kappa - 2[(\eta_e - \eta_m)/\eta_e](1 - \cos \kappa)} \right] \\ & \times \left[\left(\frac{\mu_0 H^2}{\zeta \Omega}\right) \tilde{l}_0 - 2\tilde{V} \right], \end{aligned} \tag{3.27}$$

with the dimensionless parameter κ given by

$$\kappa = \left[\frac{-4\zeta\eta_m}{(\eta_e - \eta_m)\eta_e} \frac{\zeta d^2}{\eta'} \right]^{1/2}. \tag{3.28}$$

Note that the translational velocity, (3.26), for the nonzero-spin-viscosity case contains the zero-spin-viscosity solution, (3.12), as well as additional terms which represent the effect of spin-diffusion on the flow. This separation is not as clear in the solution for the spin-velocity, (3.27).

Our solutions for the translational and spin-velocity fields are similar to those given by Condiff and Dahler¹⁹ for electrical induction flow between parallel plates. However, the interesting coupling effects between pressure gradient, body-couple, and spin/vorticity studied here in detail were not given consideration by these authors.

Figures 7–12 show representative profiles for the translational and spin-velocity, with $\partial \tilde{p}' / \partial \tilde{z} = -1$. Figures 7 and 8, respectively, show translational and spin-velocity profiles for positive and negative effective viscosities ($\eta_m / \eta = \pm 0.5$) with and without the effect of zeroth-order body-couple ($\tilde{l}_0 = \{0, 1\}$) with $\tilde{V} = 0$. When the zeroth-order body-

couple is zero the translational velocity profile is symmetric about the $\tilde{x} = 0.5$ yz -plane while the spin-velocity is antisymmetric about the same plane. The translational velocity profile is in general *not* parabolic, except for special parameter values. When \tilde{l}_0 is nonzero the symmetries about the $\tilde{x} = 0.5$ yz -plane disappear, and for the particular parameter values of Fig. 7 ($\zeta/\eta = 0.15$, $\eta'/\zeta d^2 = 0.01$, $\eta_m/\eta = -0.5$, $\tilde{l}_0 = 1$) reverse flow is possible over a small section of the gap near the $\tilde{x} = 1$ wall. Because in Figs. 7 and 8 nonzero values of \tilde{l}_0 are along the y -direction (see Fig. 1) the zeroth-order body-couple opposes the flow vorticity in the lower half of the gap, and *vice versa* “aids” the vorticity for most of the upper half. Note that even though negative magneto-viscosities are used in Fig. 7, the volumetric flow rate is positive for all parameter combinations in the figure.

Figures 9 and 10 show the effect of increasing imaginary κ on translational and spin-velocity profiles, respectively. These figures are for physical parameters equal to those of Figs. 7 and 8 ($\zeta/\eta = 0.15$, $\eta'/\zeta d^2 = 0.01$). The parameter κ is then controlled through η_m , as given in (3.28). Imaginary values of κ correspond to operating regimes to the left of α_0 in Fig. 4. Nonzero values of \tilde{l}_0 would result in removing

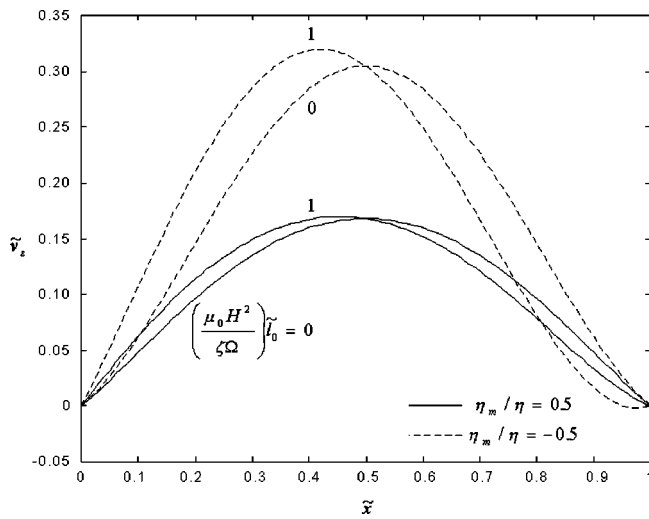


FIG. 7. Translational velocity profiles for the nonzero spin-viscosity case, Eq. (3.26). Parameter values are those of Fig. 6, with $\eta'/\zeta d^2=0.01$ and $(\mu_0 H^2/\zeta\Omega)\bar{T}_0=\{0,1\}$. Note that \bar{Q} , Eq. (3.30), is positive even for $\eta_m = -0.5$. Also note that a nonzero $(\mu_0 H^2/\zeta\Omega)\bar{T}_0$ affects the shape and symmetry of the translational velocity profile.

symmetry about the $\tilde{x}=0.5$ yz -plane, as in Figs. 7 and 8. It is apparent from Figs. 9 and 10 that the nonzero-spin-viscosity solution approaches a limiting value as $\kappa \rightarrow j\infty$. This limit is discussed further with relation to Figs. 15 and 16 and in Sec. III B 1.

As noted in Sec. III, the spin-viscosity is commonly *assumed* to be proportional to the suspending fluid viscosity η_0 , the ferrofluid volume fraction ϕ and the characteristic particle diameter L_p squared ($\eta' \propto \phi \eta_0 L_p^2$). This would imply that $\eta'/\zeta d^2 \sim (L_p/d)^2$. Considering flow of a typical ferrofluid with particle diameter $L_p \sim 10^{-8}$ m, in ducts with characteristic linear dimension $d \sim 10^{-3}$ m, this would imply that $\eta'/\zeta d^2 \sim 10^{-10}$. Instead of using this value, we have *arbitrarily* chosen to use $\eta'/\zeta d^2 \sim 10^{-2}$ in most of our figures for three reasons. First, microfluidic ferrofluid flows

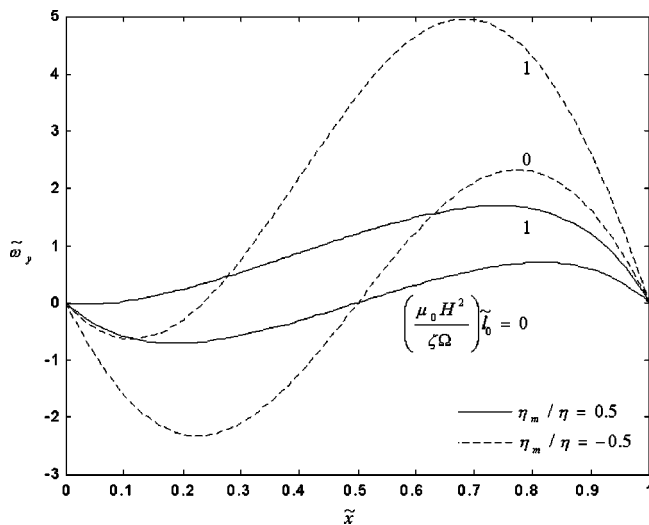


FIG. 8. Spin velocity profiles for the nonzero spin-viscosity case, Eq. (3.27). Parameter values are those of Fig. 7.

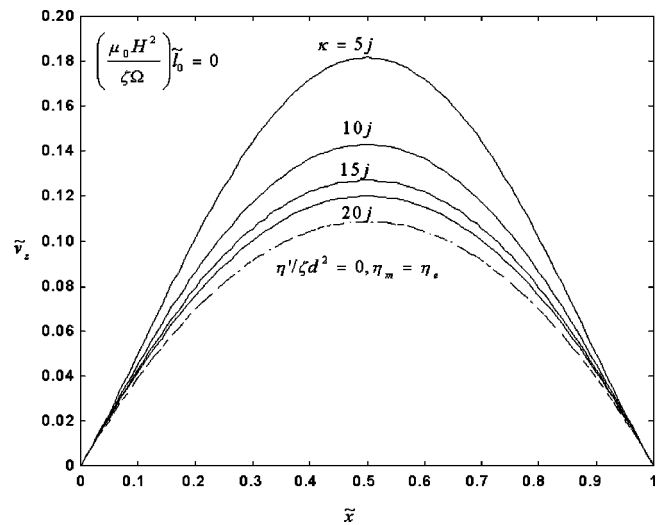


FIG. 9. Translational velocity profiles for $\zeta/\eta=0.15$, $\eta'/\zeta d^2=0.01$, $\kappa = \{5j, 10j, 15j, 20j\}$ (corresponding to $\eta_m/\eta = \{0.3725, 0.7557, 0.9335, 1.0173\}$), $\partial\bar{p}'/\partial\tilde{z} = -1$, $\bar{V} = 0$ and $(\mu_0 H^2/\zeta\Omega)\bar{T}_0 = 0$. As $\kappa \rightarrow j\infty$ the zero-spin-viscosity solution is approached, shown by the dashed line for $\eta_m = \eta_e$.

with $d \sim 10^{-6}$ m are currently being considered⁴⁰ making $\eta'/\zeta d^2 \sim 10^{-4}$. A sub-micron device would bring $\eta'/\zeta d^2$ closer to our chosen value, hence, spin-diffusion could have a profound effect on the behavior of these systems. Second, to our knowledge, it has not actually been *shown* that the intrinsic length scale L_p corresponds, *inter alia*, to the particle diameter, in contrast with the explicit proportionality of ζ on the particle diameter, quantified by (3.7).¹² As discussed by Brenner,¹² the macro-continuum description of suspensions is dependent on three distinct length scales: (i) a micro-scale dimension l , characteristic of the suspended particles, (ii) a macro-scale dimension L , determined by the apparatus constraining the flow of the suspension, and (iii) a meso-scale dimension \mathcal{L} at which the macro-continuum fields are defined from their micro-continuum analogs. It is entirely

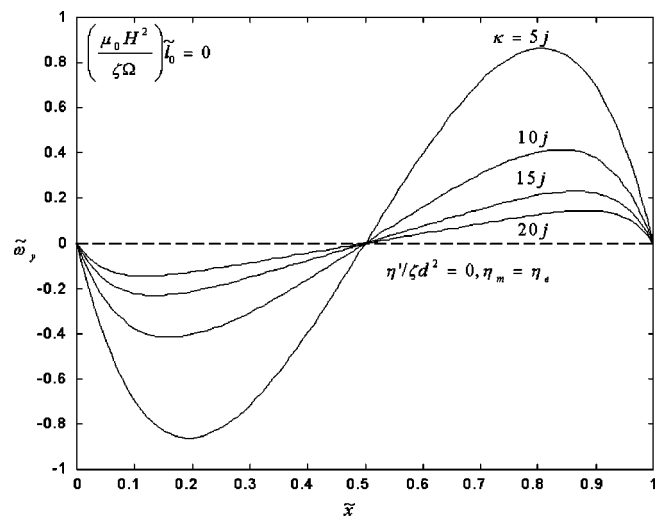


FIG. 10. Spin-velocity profiles for the nonzero-spin-viscosity case. Parameter values are those of Fig. 9.

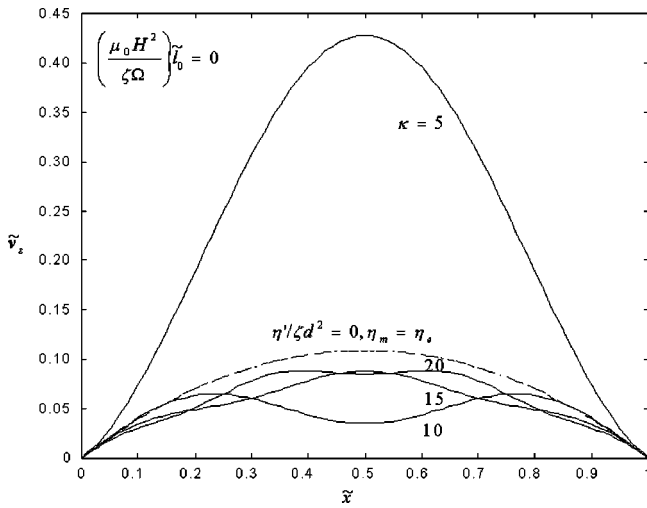


FIG. 11. Translational velocity profiles for $\zeta/\eta=0.15$, $\eta'/\zeta d^2=0.01$, $\kappa=\{5,10,15,20\}$ (corresponding to $\eta_m/\eta=\{-1.0580,2.4045,1.4972,1.3225\}$), $\partial\tilde{p}'/\partial\tilde{z}=-1$, $\tilde{V}=0$, and $(\mu_0 H^2/\zeta\Omega)\tilde{T}_0=0$. Note that the spatial period of the spatial sinusoidal oscillations and their amplitudes are functions of κ . This is discussed further in Sec. III B 3. Also note that as κ increases, the zero-spin-viscosity solution for $\eta_m = \eta_e$, shown by the dashed line, is approached.

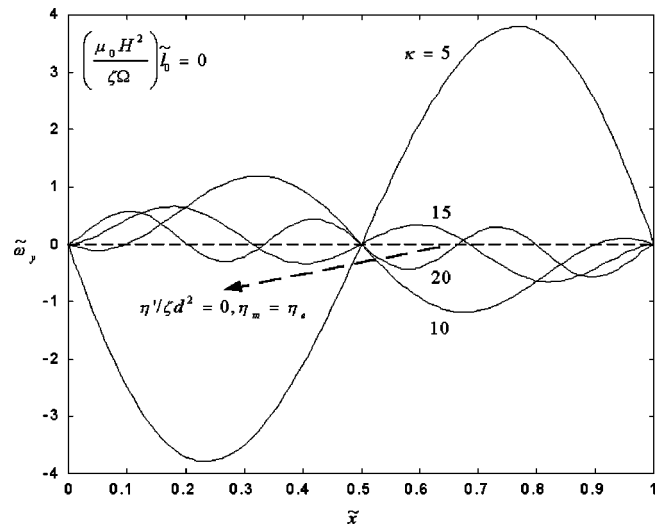


FIG. 12. Spin-velocity profiles for the nonzero-spin-viscosity case. Parameter values are those of Fig. 11.

plausible that L_p is in fact proportional to the mesoscale \mathcal{L} squared and hence much larger than expected. Indeed, experimental evidence supports this possibility.^{34,41} The micro-scale l and mesoscale \mathcal{L} are of the same magnitude only for the degenerate case of an infinite, spatially periodic particle suspension.⁴² Furthermore, to ensure equivalence between spatial and ensemble averages, it is commonly required that $l \ll \mathcal{L}$, hence it is possible that the spin-viscosity is much larger than is commonly assumed. Finally, we have chosen $\eta'/\zeta d^2 \sim 10^{-2}$ to emphasize the effect of spin-diffusion in ferrofluid flows, in keeping with the goal of this contribution.

Figures 11 and 12 show the effect of increasing real κ on translational and spin-velocity profiles, respectively. As with Figs. 7–10, Figs. 11 and 12 are for physical parameters $\zeta/\eta=0.15$ and $\eta'/\zeta d^2=0.01$. The parameter κ is controlled through the effective viscosity η_m . These profiles correspond to operating regimes to the right of α_0 in Fig. 4. These profiles for real κ predict spatially oscillating translational and spin-velocity profiles even in the absence of zeroth-order body-couple effects. This is not predicted by the zero-spin-viscosity solution. As with Figs. 9 and 10, the nonzero-spin-viscosity solution seems to approach limiting behavior as $\kappa \rightarrow \infty$. Here the average profile approaches a limiting value as the number of periods of oscillation and the oscillation amplitude change.

The corresponding vorticity is

$$\begin{aligned} \tilde{\Omega}_y(\tilde{x}) = & \frac{\eta}{2\eta_m} \left[1 - 2\tilde{x} + \frac{(\eta_e - \eta_m)}{\eta_e} \frac{(1 + \cos \kappa) \sin \kappa \tilde{x} - \sin \kappa \cos \kappa \tilde{x}}{\sin \kappa} \right] \frac{\partial \tilde{p}'}{\partial \tilde{z}} - \tilde{V} \\ & + \left[\frac{(\eta_e - \eta_m)}{2\eta_e} \frac{(1 - \cos \kappa)(2 - \kappa \sin \kappa \tilde{x}) - \kappa \sin \kappa \cos \kappa \tilde{x}}{\kappa \sin \kappa - 2[(\eta_e - \eta_m)/\eta_e](1 - \cos \kappa)} \right] \left[\left(\frac{\mu_0 H^2}{\zeta \Omega} \right) \tilde{T}_0 - 2\tilde{V} \right]. \end{aligned} \quad (3.29)$$

Because we are interested in situations for which flow reversal might occur, corresponding to forward or backward pumping in the presence of a pressure gradient, we calculate the volumetric flow rate,

$$\begin{aligned} \tilde{Q} = & -\frac{\eta}{12\eta_m} \left\{ 1 - 6 \frac{\eta_e - \eta_m}{\kappa^2 \eta_e} \left[2 - \frac{\kappa(1 + \cos \kappa)}{\sin \kappa} \right] \right\} \frac{\partial \tilde{p}'}{\partial \tilde{z}} \\ & + \frac{1}{2} \tilde{V}. \end{aligned} \quad (3.30)$$

Note that as in the zero spin-viscosity solution, the zeroth-order body-couple term, \tilde{T}_0 , has no effect on the volumetric flow rate. Figure 13 shows that this expression for the volu-

metric flow is discontinuous, as in the zero-spin-viscosity case, (3.21), but in this case the discontinuity occurs at a nonzero value of the effective viscosity η_m . In fact, as Fig. 14 shows, the nonzero-spin-viscosity solution predicts a multitude of such discontinuities (when $\kappa = n\pi$ with n an even integer). Finding conditions for which the volumetric flow rate is zero involves finding roots of (3.30) with respect to the effective viscosity (in general this must be done numerically), and in turn determining the required magnetic field for a specified field frequency through (3.15) and (2.32).

As mentioned before, the translational and spin-velocity profiles of Figs. 9–12 seem to show limiting behavior as the

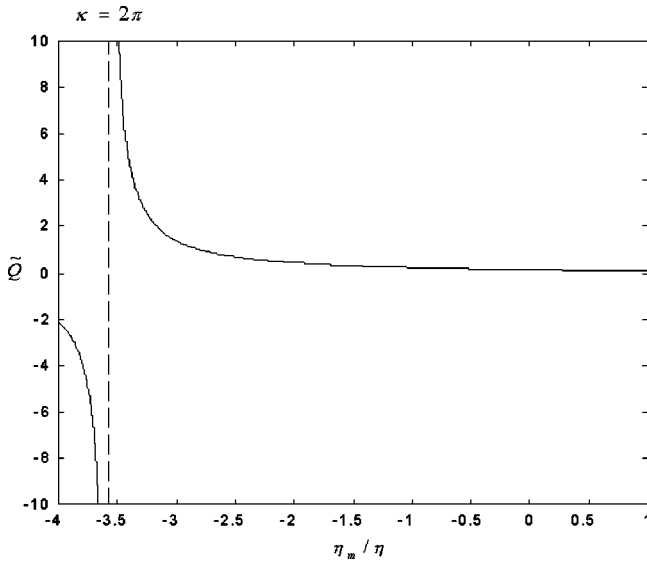


FIG. 13. Scaled volumetric flow rate as a function of η_m for the nonzero-spin-viscosity solution. One flow reversal for $\eta_m \sim -3.6$ is shown. This corresponds to $\kappa = 2\pi$ [η_m in that case is given by Eq. (3.39)]. Parameter values are $\zeta/\eta = 0.15$, $\eta'/\zeta d^2 = 0.01$, $\partial\tilde{p}'/\partial\tilde{z} = -1$, and $\tilde{V} = 0$.

magnitude of κ increases. Because the physical properties (namely the vortex and spin viscosities) are held constant in these figures, we must let η_m approach η_e , which is not possible in practice as it requires infinite magnetic fields. Figures 15–18 show analogous plots in which the vortex and effective viscosities are held constant while the spin viscosity approaches zero ($\eta'/\zeta d^2 \rightarrow 0$). Figures 15 and 16 correspond to imaginary κ ($\zeta/\eta = 0.15$, $\eta_m/\eta = 0.5$) whereas Figs. 17 and 18 correspond to real κ ($\zeta/\eta = 0.15$, $\eta_m/\eta = -0.5$). In all cases the velocity profiles seem to approach

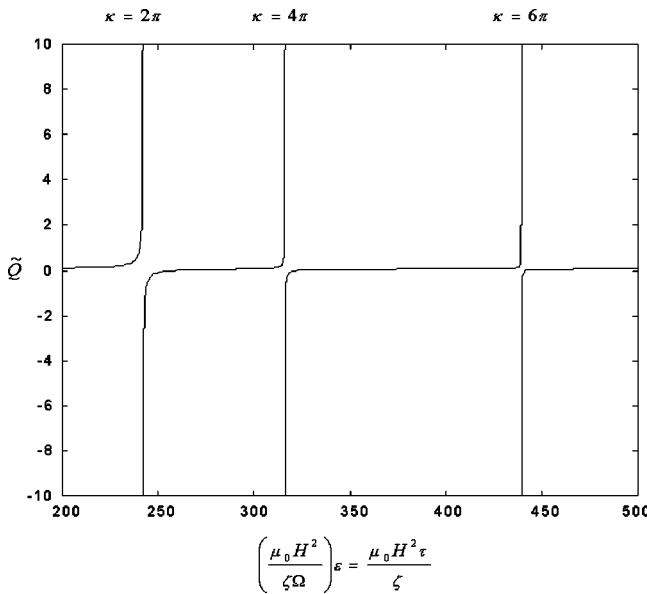


FIG. 14. Scaled volumetric flow rate as a function of $(\mu_0 H^2 / \zeta \Omega) \epsilon = \mu_0 H^2 \tau / \zeta$. The first three discontinuities in flow rate are shown, corresponding to $\kappa = \{2\pi, 4\pi, 6\pi\}$. Parameter values are the same as in Fig. 13. These flow discontinuities correspond to fields of $\mu_0 H \sim \{0.37\text{T}, 0.42\text{T}, 0.49\text{T}\}$ (for $\tau = 10^{-5}$ s and $\eta = 0.03$ Nsm $^{-2}$).

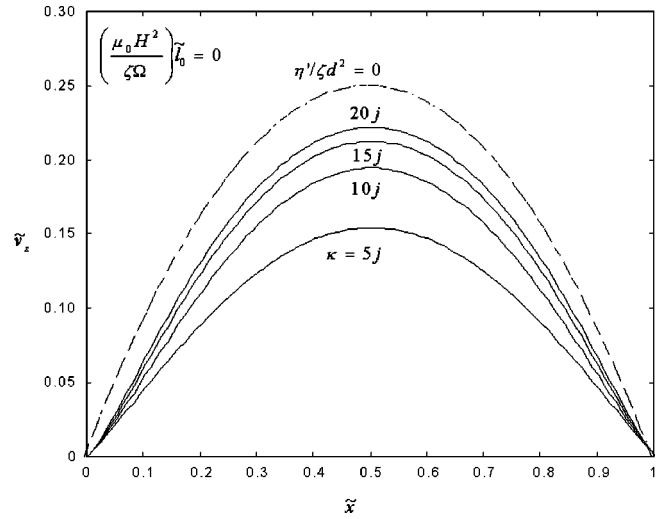


FIG. 15. Translational velocity profiles for $\zeta/\eta = 0.15$, $\eta_m/\eta = 0.5$, and $\kappa = \{5j, 10j, 15j, 20j\}$ (corresponding to $\eta'/\zeta d^2 = \{1.6 \times 10^{-2}, 4 \times 10^{-3}, 2 \times 10^{-3}, 1 \times 10^{-3}\}$), $\partial\tilde{p}'/\partial\tilde{z} = -1$, $\tilde{V} = 0$, and $(\mu_0 H^2 / \zeta \Omega) \tilde{t}_0 = 0$. The dashed line corresponds to the zero-spin-viscosity solution.

the zero-spin-viscosity solution (shown by the dashed profile in all figures). This can be easily shown for imaginary κ , and is the subject of the following section. For real κ the analysis is more involved as discontinuities in the flow profiles occur for $\kappa = n\pi$ (even n), as mentioned above.

1. Limiting behavior as $\kappa \rightarrow j\infty$

As noted above in relation to Figs. 9, 10, 15, and 16, the nonzero-spin-viscosity solution seems to approach a limit as imaginary κ goes to infinity. In fact, Figs. 15 and 16 suggest that this limit corresponds to the zero-spin-viscosity solution. Here we show that this is rigorously the case by taking the limit $\kappa \rightarrow j\infty$ in (3.28), while holding ζ , η , and η_m constant (effectively letting $\eta'/\zeta d^2 \rightarrow 0$). The resulting limits corresponding to (3.26)–(3.30) are

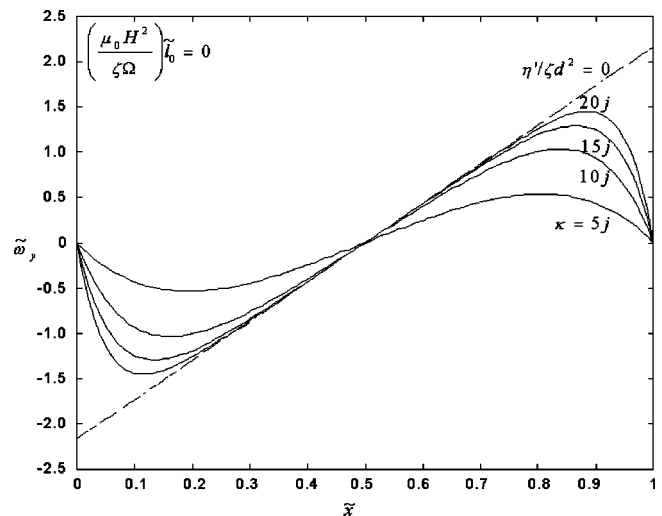


FIG. 16. Spin velocity profiles for the nonzero-spin-viscosity case. Parameter values are those of Fig. 15. The dashed line corresponds to the zero-spin-viscosity solution.

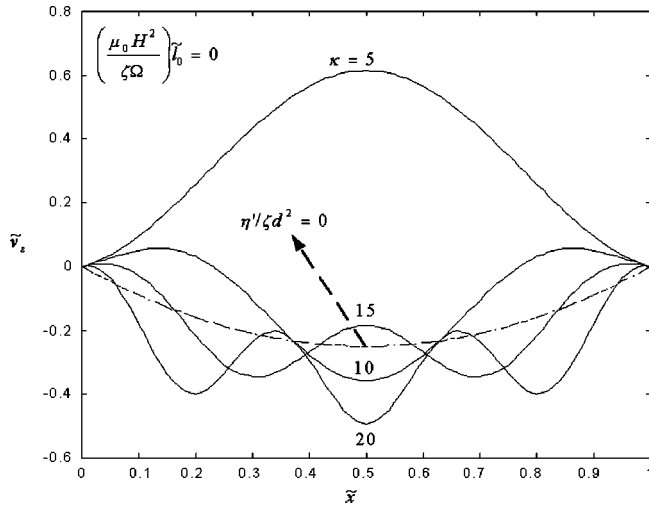


FIG. 17. Translational velocity profiles for $\zeta/\eta=0.15$, $\eta_m/\eta=-0.5$, and $\kappa=\{5,10,15,20\}$ (corresponding to $\eta'/\zeta d^2=\{6\times 10^{-2},2\times 10^{-2},7\times 10^{-4},4\times 10^{-4}\}$), $\partial\tilde{p}'/\partial\tilde{z}=-1$, $\tilde{V}=0$, and $(\mu_0 H^2/\zeta\Omega)\tilde{I}_0=0$. The dashed line corresponds to the zero-spin-viscosity solution.

$$\lim_{\kappa \rightarrow j\infty} \tilde{v}_z(\tilde{x}) = \frac{\tilde{x}(\tilde{x}-1)\eta}{2\eta_m} \frac{\partial\tilde{p}'}{\partial\tilde{z}} + \tilde{V}\tilde{x}, \tag{3.31}$$

for the translational velocity,

$$\lim_{\kappa \rightarrow j\infty} \tilde{\omega}_y(\tilde{x}) = \begin{cases} \frac{(\eta_e - \eta_m)}{4\zeta} \left[\frac{1-2\tilde{x}}{\eta_m/\eta} \frac{\partial\tilde{p}'}{\partial\tilde{z}} + \left(\frac{\mu_0 H^2}{\zeta\Omega} \right) \tilde{I}_0 - 2\tilde{V} \right], & \text{if } 0 < \tilde{x} < 1, \\ 0, & \text{if } \tilde{x} = \{0,1\}, \end{cases} \tag{3.32}$$

for the spin-velocity,

$$\lim_{\kappa \rightarrow j\infty} \tilde{\Omega}_y(\tilde{x}) = \frac{(1-2\tilde{x})\eta}{2\eta_m} \frac{\partial\tilde{p}'}{\partial\tilde{z}} - \tilde{V}, \tag{3.33}$$

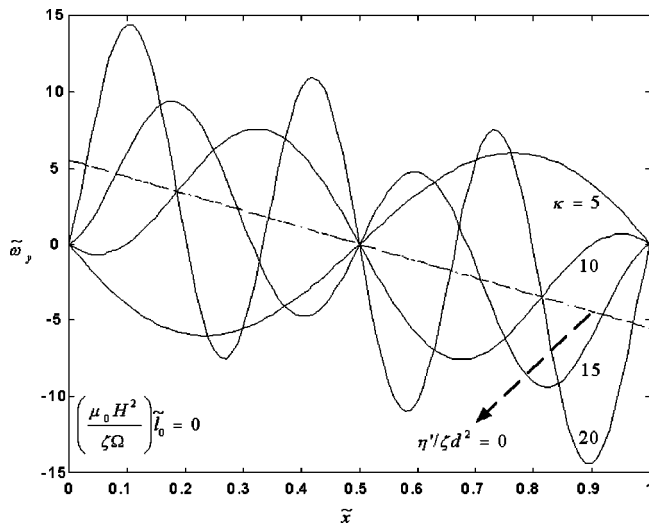


FIG. 18. Spin-velocity profiles for the nonzero-spin-viscosity case. Parameter values are those of Fig. 17. The dashed line corresponds to the zero-spin-viscosity solution.

for the vorticity, and

$$\lim_{\kappa \rightarrow j\infty} \tilde{Q} = -\frac{\eta}{12\eta_m} \frac{\partial\tilde{p}'}{\partial\tilde{z}} + \frac{1}{2}\tilde{V}, \tag{3.34}$$

for the volumetric flow rate. These results are identical to those for the zero-spin-viscosity solution [(3.12), (3.19), (3.20), and (3.21)], except for the spin-velocity solution, (3.32), which is equivalent to the zero-spin-viscosity solution with a discontinuity at $\tilde{x}=0$ and $\tilde{x}=1$ to satisfy the imposed zero-spin-velocity boundary condition, (3.25b).

We point out that (3.31)–(3.34) are only applicable for infinite imaginary κ , which requires positive, nonzero effective viscosities ($\eta_m > 0$) and hence the singularity at $\eta_m = 0$ in the zero-spin-viscosity solution does not apply.

2. Flow profiles as $\eta_m \rightarrow 0$

As noted in Sec. III A, neglecting spin-viscosity effects results in translational and spin velocity profiles which become nonphysical when the parameter η_m , the so-called magnetoviscosity of the ferrofluid, is zero. Here we show how the solution for the translational and spin-velocity remains physical in this limit when the effects of spin viscosity are retained in the internal angular momentum equation.

When the limit $\eta_m \rightarrow 0$ is taken [by noting the explicit dependence of κ on η_m , given in (3.28)], the resulting translational and spin-velocity profiles are

$$\begin{aligned} \lim_{\eta_m \rightarrow 0} \tilde{v}_z(\tilde{x}) = & -\frac{\eta}{\eta_e} \left[\frac{\tilde{x}(1-\tilde{x})}{2} + \frac{\tilde{x}^2(1-\tilde{x})^2}{6\eta_e/\zeta} \left(\frac{\zeta d^2}{\eta'} \right) \right] \frac{\partial\tilde{p}'}{\partial\tilde{z}} \\ & + \tilde{V}\tilde{x} - \frac{1}{2} \frac{\zeta}{\eta_e} \frac{\tilde{x}(1-\tilde{x})(2\tilde{x}-1)}{3(\eta'/\zeta d^2) + (\zeta/\eta_e)} \\ & \times \left[\left(\frac{\mu_0 H^2}{\zeta\Omega} \right) \tilde{I}_0 - 2\tilde{V} \right], \end{aligned} \tag{3.35}$$

and

$$\begin{aligned} \lim_{\eta_m \rightarrow 0} \tilde{\omega}_y(\tilde{x}) = & -\frac{\tilde{x}(1-\tilde{x})(2\tilde{x}-1)\eta}{6\eta_e} \left(\frac{\zeta d^2}{\eta'} \right) \frac{\partial\tilde{p}'}{\partial\tilde{z}} \\ & + \frac{3}{2} \frac{\tilde{x}(1-\tilde{x})}{3(\eta'/\zeta d^2) + (\zeta/\eta_e)} \\ & \times \left[\left(\frac{\mu_0 H^2}{\zeta\Omega} \right) \tilde{I}_0 - 2\tilde{V} \right]. \end{aligned} \tag{3.36}$$

The vorticity field corresponding to this translational velocity field is

$$\lim_{\eta_m \rightarrow 0} \tilde{\Omega}_y(\tilde{x}) = \frac{\eta}{\eta_e} \left[\frac{(1-2\tilde{x})}{2} + \frac{\tilde{x}(1-2\tilde{x})(1-\tilde{x})}{3\eta_e/\zeta} \left(\frac{\zeta d^2}{\eta'} \right) \right] \times \frac{\partial \tilde{p}'}{\partial \tilde{z}} - \tilde{V} - \frac{1}{2} \frac{\zeta}{\eta_e} \frac{1-6\tilde{x}(1-\tilde{x})}{3(\eta'/\zeta d^2) + (\zeta/\eta_e)} \times \left[\left(\frac{\mu_0 H^2}{\zeta \Omega} \right) \tilde{I}_0 - 2\tilde{V} \right]. \tag{3.37}$$

Finally, the volumetric flow rate of the ferrofluid is given in this case by

$$\lim_{\eta_m \rightarrow 0} \tilde{Q} = -\frac{1}{12} \frac{\eta}{\eta_e} \left[1 + \frac{1}{15} \frac{\zeta}{\eta_e} \left(\frac{\zeta d^2}{\eta'} \right) \right] \frac{\partial \tilde{p}'}{\partial \tilde{z}} + \frac{1}{2} \tilde{V}. \tag{3.38}$$

Equations (3.35)–(3.38) show that the nonzero-spin-viscosity solutions remain finite for conditions where $\eta_m = 0$. However, it is clearly evident that these limiting solutions still predict very large velocities for small values of the spin-viscosity, η' . The predicted limiting flows as $\eta'/\zeta d^2 \rightarrow 0$, however, are very different from those predicted by the zero-spin-viscosity solution. For example, (3.35) shows that the nonzero-spin-viscosity solution predicts a flow profile described by a fourth-order polynomial in \tilde{x} for conditions where $\eta_m \rightarrow 0$, $\eta'/\zeta d^2 \rightarrow 0$, whereas the zero-spin-viscosity solution, (3.12), predicts a flow profile described by a second-order polynomial in \tilde{x} .

3. Limiting behavior as $\kappa \rightarrow n\pi$, $n=1,2,3$

Inspection of the translational and spin-velocities, (3.26) and (3.27), as well as the volumetric flow rate, (3.30), shows that the limit $\kappa \rightarrow n\pi$ may result in infinite flow rates. This was also shown graphically for the volumetric flow rates in Figs. 13 and 14 and mentioned in relation to flow behavior as κ approaches real infinity, Figs. 11, 12, 17, and 18. For a given ferrofluid, making κ approach $n\pi$ requires control of the effective viscosity. Using (3.28), we find that having $\kappa = n\pi$ requires

$$\eta_m = \frac{\eta_e}{[1 - (4\zeta/n^2 \pi^2 \eta_e) (\zeta d^2/\eta')]} \tag{3.39}$$

Upon taking the limit $\kappa \rightarrow n\pi$ of (3.26)–(3.30), we find that the flow fields remain finite for odd n but may become unbounded for even n .

(a) *Odd n.* Limiting behavior as $\kappa \rightarrow n\pi$, odd n , are easily found. They are

$$\lim_{\substack{\kappa \rightarrow n\pi \\ n \text{ odd}}} \tilde{v}_z(\tilde{x}) = -\frac{\eta}{2\eta_m} \left[\tilde{x}(1-\tilde{x}) - \frac{(\eta_e - \eta_m) \sin n\pi\tilde{x}}{\eta_e} \frac{\partial \tilde{p}'}{\partial \tilde{z}} \right] + \tilde{V}\tilde{x} - \frac{1-2\tilde{x} - \cos(n\pi\tilde{x})}{4} \times \left[\left(\frac{\mu_0 H^2}{\zeta \Omega} \right) \tilde{I}_0 - 2\tilde{V} \right], \tag{3.40}$$

for the translational velocity profile,

$$\lim_{\substack{\kappa \rightarrow n\pi \\ n \text{ odd}}} \tilde{\omega}_y(\tilde{x}) = \frac{\eta(\eta_e - \eta_m)}{4\zeta\eta_m} (1-2\tilde{x} - \cos n\pi\tilde{x}) \frac{\partial \tilde{p}'}{\partial \tilde{z}} + \frac{\eta_e}{8\zeta} n\pi \sin n\pi\tilde{x} \left[\left(\frac{\mu_0 H^2}{\zeta \Omega} \right) \tilde{I}_0 - 2\tilde{V} \right], \tag{3.41}$$

for the spin-velocity profile,

$$\lim_{\substack{\kappa \rightarrow n\pi \\ n \text{ odd}}} \tilde{\Omega}_y(\tilde{x}) = -\frac{\eta}{2\eta_m} \left[2\tilde{x} - 1 + \frac{(\eta_e - \eta_m) \cos(n\pi\tilde{x})}{\eta_e} \right] \frac{\partial \tilde{p}'}{\partial \tilde{z}} - \tilde{V} - \frac{2-n\pi \sin n\pi\tilde{x}}{4} \left[\left(\frac{\mu_0 H^2}{\zeta \Omega} \right) \tilde{I}_0 - 2\tilde{V} \right], \tag{3.42}$$

for the flow vorticity, and

$$\lim_{\substack{\kappa \rightarrow n\pi \\ n \text{ odd}}} \tilde{Q} = -\frac{\eta}{12\eta_m} \left[1 - \frac{12}{n^2 \pi^2} \frac{(\eta_e - \eta_m)}{\eta_e} \right] \frac{\partial \tilde{p}'}{\partial \tilde{z}} + \frac{1}{2} \tilde{V}, \tag{3.43}$$

for the volumetric flow rate.

(b) *Even n.* For even n we find that the translational and spin-velocity fields become infinite. The condition $\kappa = n\pi$ for even n therefore seems to indicate some form of resonance in the problem.

We can still find the predicted limiting behavior for the flow by letting $\kappa \rightarrow n\pi + \delta$ and then considering the limit of small δ . The result is then expanded in the parameter δ , keeping only the leading-order $O(\delta^{-1})$ and $O(1)$ terms. The resulting translational velocity is

$$\lim_{\substack{\kappa \rightarrow n\pi + \delta \\ \delta \rightarrow 0}} \tilde{v}_z(\tilde{x}) = -\frac{(\eta_e - \eta_m)\eta}{\eta_e \eta_m} \frac{1 - \cos n\pi\tilde{x}}{n\pi} \delta^{-1} \frac{\partial \tilde{p}'}{\partial \tilde{z}} - \left[\frac{\tilde{x}(1-\tilde{x})\eta}{2\eta_m} + \frac{\eta(\eta_e - \eta_m)}{2\eta_e \eta_m} \frac{n\pi(2\tilde{x}-1)(\sin n\pi\tilde{x}) - 2(1 - \cos n\pi\tilde{x})}{n^2 \pi^2} \right] \times \frac{\partial \tilde{p}'}{\partial \tilde{z}} + \tilde{V}\tilde{x} + \left[\frac{(\eta_e - \eta_m) \sin n\pi\tilde{x}}{2\eta_e} \frac{1}{n\pi} \right] \left[\left(\frac{\mu_0 H^2}{\zeta \Omega} \right) \tilde{I}_0 - 2\tilde{V} \right]. \tag{3.44}$$

The spin-velocity is

$$\lim_{\substack{\kappa \rightarrow n\pi + \delta \\ \delta \rightarrow 0}} \tilde{\omega}_y(\tilde{x}) = \frac{(\eta_e - \eta_m)\eta \sin n\pi\tilde{x}}{2\zeta\eta_m} \delta^{-1} \frac{\partial \tilde{p}'}{\partial \tilde{z}} - \frac{(\eta_e - \eta_m)\eta}{4\zeta\eta_m} (2\tilde{x} - 1)(1 - \cos n\pi\tilde{x}) \frac{\partial \tilde{p}'}{\partial \tilde{z}} + \frac{(\eta_e - \eta_m)(1 - \cos n\pi\tilde{x})}{4\zeta} \left[\left(\frac{\mu_0 H^2}{\zeta\Omega} \right) \tilde{l}_0 - 2\tilde{V} \right]. \tag{3.45}$$

The vorticity of the flow is

$$\lim_{\substack{\kappa \rightarrow n\pi + \delta \\ \delta \rightarrow 0}} \tilde{\Omega}_y(\tilde{x}) = -\frac{(\eta_e - \eta_m)\eta \sin n\pi\tilde{x}}{\eta_e\eta_m} \delta^{-1} \frac{\partial \tilde{p}'}{\partial \tilde{z}} + \frac{(1 - 2\tilde{x})\eta}{2\eta_m} \frac{\partial \tilde{p}'}{\partial \tilde{z}} + \frac{\eta(\eta_e - \eta_m)}{2\eta_e\eta_m} \times \frac{2\tilde{x} \sin n\pi\tilde{x} + n\pi(2\tilde{x} - 1)(\cos n\pi\tilde{x}) - 2 \sin n\pi\tilde{x}}{n\pi} \frac{\partial \tilde{p}'}{\partial \tilde{z}} - \tilde{V} - \left[\frac{(\eta_e - \eta_m)}{2\eta_e} \cos n\pi\tilde{x} \right] \left[\left(\frac{\mu_0 H^2}{\zeta\Omega} \right) \tilde{l}_0 - 2\tilde{V} \right]. \tag{3.46}$$

Finally, the volumetric flow rate for these conditions is

$$\lim_{\substack{\kappa \rightarrow n\pi + \delta \\ \delta \rightarrow 0}} \tilde{Q} = \frac{\eta(\eta_e - \eta_m)}{n\pi\eta_e\eta_m} \delta^{-1} \frac{\partial \tilde{p}'}{\partial \tilde{z}} - \frac{\eta}{12\eta_m} \times \left\{ 1 - 24 \frac{(\eta_e - \eta_m)}{n^2\pi^2\eta_e} \right\} \frac{\partial \tilde{p}'}{\partial \tilde{z}} + \frac{1}{2} \tilde{V}. \tag{3.47}$$

Note that in all these expressions, the leading-order term, of order $\mathcal{O}(\delta^{-1})$, is proportional to the dynamic pressure gradient $\partial \tilde{p}' / \partial \tilde{z}$.

4. Limiting behavior as $\eta_m \rightarrow \pm\infty$

As discussed in Sec. III A, the effective viscosity η_m is a discontinuous function of the parameter $\alpha \equiv \langle \tilde{l}_y \rangle_1 / \tilde{\omega}_y$ in the assumed linear form of the body-couple density field, (2.38). Particularly, it is possible for η_m to achieve infinite values under well characterized conditions, namely those satisfying (3.14). The limiting behavior of the translational and spin-velocity equations, and their consequences, in the limit $\eta_m \rightarrow \pm\infty$ is therefore interesting.

These limits are easily evaluated to be

$$\lim_{\eta_m \rightarrow \pm\infty} \tilde{v}_z(\tilde{x}) = \frac{\eta}{2\eta_e} \left[\frac{(1 + \cos \kappa)(1 - \cos \kappa\tilde{x}) - \sin \kappa \sin \kappa\tilde{x}}{\kappa \sin \kappa} \right] \frac{\partial \tilde{p}'}{\partial \tilde{z}} + \tilde{V}\tilde{x} - \frac{1}{4} \left[\frac{(1 - \cos \kappa)(1 - 2\tilde{x} - \cos \kappa\tilde{x}) + \sin \kappa \sin \kappa\tilde{x}}{1 - \cos \kappa} \right] \times \left[\left(\frac{\mu_0 H^2}{\zeta\Omega} \right) \tilde{l}_0 - 2\tilde{V} \right], \tag{3.48}$$

and

$$\lim_{\eta_m \rightarrow \pm\infty} \tilde{\omega}_y(\tilde{x}) = -\frac{\eta}{4\zeta} \left[\frac{\sin \kappa(1 - 2\tilde{x} - \cos \kappa\tilde{x}) + (1 + \cos \kappa) \sin \kappa\tilde{x}}{\sin \kappa} \right] \frac{\partial \tilde{p}'}{\partial \tilde{z}} + \frac{\eta_e}{8\zeta} \left[\frac{\kappa \sin \kappa\tilde{x}(1 - \cos \kappa) - \kappa \sin \kappa(1 - \cos \kappa\tilde{x})}{1 - \cos \kappa} \right] \times \left[\left(\frac{\mu_0 H^2}{\zeta\Omega} \right) \tilde{l}_0 - 2\tilde{V} \right], \tag{3.49}$$

with the dimensionless parameter κ reducing to

$$\kappa = \left[\frac{4\zeta}{\eta_e} \frac{\zeta d^2}{\eta'} \right]^{1/2}. \tag{3.50}$$

These limits show that even though η_m is a discontinuous function, the ferrofluid behavior does not undergo a discontinuity as the critical value of α , (3.14), is approached. This should have been expected when one considers that the parameter η_m is fictitious [the original governing equations, (3.4) and (3.6), had no explicit dependence on it]. It was only introduced by analogy with the classical solution for pressure-driven flow between parallel plates.³⁹

The vorticity corresponding to the translational velocity field in this limit is

$$\lim_{\eta_m \rightarrow \pm\infty} \tilde{\Omega}_y(\tilde{x}) = -\frac{\eta}{2\eta_e} \left[\frac{(1 + \cos \kappa) \sin \kappa\tilde{x} - \sin \kappa \cos \kappa\tilde{x}}{\sin \kappa} \right] \frac{\partial \tilde{p}'}{\partial \tilde{z}} - \tilde{V} - \frac{1}{4} \left[\frac{(1 - \cos \kappa)(2 - \kappa \sin \kappa\tilde{x}) - \kappa \sin \kappa \cos \kappa\tilde{x}}{1 - \cos \kappa} \right] \times \left[\left(\frac{\mu_0 H^2}{\zeta\Omega} \right) \tilde{l}_0 - 2\tilde{V} \right]. \tag{3.51}$$

The volumetric flow rate is

$$\lim_{\eta_m \rightarrow \pm\infty} \bar{Q} = -\frac{1}{2} \frac{\eta}{\kappa^2 \eta_e} \left[2 - \frac{\kappa(1 + \cos \kappa)}{\sin \kappa} \right] \frac{\partial \tilde{p}'}{\partial \tilde{z}} + \frac{1}{2} \tilde{V}. \tag{3.52}$$

C. Nonzero-spin-viscosity solution (spin/vorticity matching at boundaries)

As discussed in Sec. I A, there is still debate over the correct boundary condition for the spin velocity. In the previous section we have studied the results for the spin–no-slip

boundary condition in detail. In this section we present the general solutions for the spin/vorticity matching boundary condition, (1.22), corresponding to zero antisymmetric stress at fluid boundaries. The imposed boundary conditions for this section are then

$$\tilde{v}_z(0) = 0, \quad \tilde{v}_z(1) = \tilde{V}, \tag{3.53a}$$

$$\tilde{\omega}_y(0) = \frac{1}{2} \tilde{\Omega}_y(0), \quad \tilde{\omega}_y(1) = \frac{1}{2} \tilde{\Omega}_y(1). \tag{3.53b}$$

The resulting translational velocity field is

$$\begin{aligned} \tilde{v}_z(\tilde{x}) = & -\frac{\tilde{x}(1-\tilde{x})\eta}{2\eta_m} \frac{\partial \tilde{p}'}{\partial \tilde{z}} + \frac{(\eta-\eta_m)}{2\eta_m} \frac{\partial \tilde{p}'}{\partial \tilde{z}} \left[\frac{\sin \kappa \sin \kappa \tilde{x} - (1 + \cos \kappa)(1 - \cos \kappa \tilde{x})}{\kappa \sin \kappa} \right] + \tilde{V} \tilde{x} \\ & + \frac{1}{2} \left\{ \frac{(\eta_e - \eta_m)}{\eta} \left(\frac{\mu_0 H^2}{\zeta \Omega} \right) \tilde{T}_0 - \frac{\eta - \eta_m}{\eta} 2\tilde{V} \right\} \left[\frac{\sin \kappa \sin \kappa \tilde{x} + (1 - \cos \kappa)(1 - 2\tilde{x} - \cos \kappa \tilde{x})}{\kappa \sin \kappa - [2(\eta - \eta_m)/\eta](1 - \cos \kappa)} \right], \end{aligned} \tag{3.54}$$

which is very similar to (3.26), for the spin–no-slip boundary condition. The spin-velocity for this flow is

$$\begin{aligned} \tilde{\omega}_y(x) = & \frac{\eta(\eta_e - \eta_m)}{4\zeta\eta_m} \frac{\partial \tilde{p}'}{\partial \tilde{z}} \left\{ 1 - 2\tilde{x} + \frac{(\eta - \eta_m)\eta_e}{\eta(\eta_e - \eta_m)} \left[\frac{(1 + \cos \kappa)\sin \kappa \tilde{x}}{\sin \kappa} - \cos \kappa \tilde{x} \right] \right\} - \frac{1}{2} \tilde{V} \\ & - \frac{1}{4} \left\{ \frac{(\eta_e - \eta_m)}{\eta} \left(\frac{\mu_0 H^2}{\zeta \Omega} \right) \tilde{T}_0 - \frac{\eta - \eta_m}{\eta} 2\tilde{V} \right\} \left[\frac{(1 - \cos \kappa)[(\eta_e/\zeta)\kappa \sin \kappa \tilde{x} - 2] + \kappa \sin \kappa [(\eta_e/\zeta)\cos \kappa \tilde{x} - (\eta/\zeta)]}{\kappa \sin \kappa - 2[(\eta - \eta_m)/\eta](1 - \cos \kappa)} \right], \end{aligned} \tag{3.55}$$

again very similar to the corresponding spin–no-slip boundary condition solution, (3.27).

The vorticity corresponding to this predicted translational velocity profile is

$$\begin{aligned} \tilde{\Omega}_y(\tilde{x}) = & \frac{(1-2\tilde{x})\eta}{2\eta_m} \frac{\partial \tilde{p}'}{\partial \tilde{z}} - \frac{(\eta-\eta_m)}{2\eta_m} \frac{\partial \tilde{p}'}{\partial \tilde{z}} \left[\frac{\sin \kappa \cos \kappa \tilde{x} - (1 + \cos \kappa)\sin \kappa \tilde{x}}{\sin \kappa} \right] - \tilde{V} \\ & - \frac{1}{2} \left\{ \frac{(\eta_e - \eta_m)}{\eta} \left(\frac{\mu_0 H^2}{\zeta \Omega} \right) \tilde{T}_0 - \frac{\eta - \eta_m}{\eta} 2\tilde{V} \right\} \left[\frac{\kappa \sin \kappa \cos \kappa \tilde{x} - (1 - \cos \kappa)(2 - \kappa \sin \kappa \tilde{x})}{\kappa \sin \kappa - [2(\eta - \eta_m)/\eta](1 - \cos \kappa)} \right], \end{aligned} \tag{3.56}$$

and the volumetric flow rate is

$$\begin{aligned} \bar{Q} = & -\frac{\eta}{12\eta_m} \frac{\partial \tilde{p}'}{\partial \tilde{z}} \left(1 - 6 \frac{\eta - \eta_m}{\kappa^2 \eta} \left(2 - \frac{\kappa(1 + \cos \kappa)}{\sin \kappa} \right) \right) \\ & + \frac{1}{2} \tilde{V}. \end{aligned} \tag{3.57}$$

The translational and spin-velocity profiles predicted using the spin/vorticity matching boundary condition on the spin-velocity are qualitatively similar to those for the spin–no-slip solution, except that the spin-velocity is now nonzero at the walls. Figures similar to Figs. 7–18 can be produced for the spin/vorticity matching solution, but do not provide any additional physical intuition. Finally, the spin/vorticity

matching solution possesses all the interesting limits of the spin–no-slip solution, with only minor changes in the coefficients in the resulting expressions. For these reasons and in the interest of brevity, we do not present these limits here.

IV. FORCE ON THE UPPER PLATE

The force on the bounding plates has two components: (i) surface excess magnetic force due to rapid changes in magnetic properties at the wall–fluid interface, and (ii) viscous traction. In general, both must be accounted for when deriving expressions for the experimental force required to move a given section of a continuum-electromechanical system.

A. Surface-excess magnetic force

The surface-excess magnetic force at the wall–fluid interface may be conveniently obtained by evaluating the jump in the “magnetic stress” tensor (or “Maxwell stress”) across the wall–fluid interface. Use of this mathematical artifice circumvents the need to know the exact distribution of magnetic fields in this region with rapidly varying magnetic properties. The Maxwell stress applicable to incompressible ferrofluid suspensions is given by^{14,43}

$$\mathbf{T}^M = \mathbf{BH} - \frac{1}{2} \mu_0 H^2 \mathbf{I}. \tag{4.1}$$

The z -directed surface-excess magnetic force per unit area on the upper plate, f_z^M , is given by the jump in the xz -component of the Maxwell stress

$$\begin{aligned} f_z^M &= T_{xz}^M(x=d^+) - T_{xz}^M(x=d^-) \\ &= (B_x H_z)|_{x=d^+} - (B_x H_z)|_{x=d^-}. \end{aligned} \tag{4.2}$$

However, the jump conditions on the magnetoquasistatic field with no surface current at $x=d$ require that the normal component of \mathbf{B} , B_x , and the tangential component of \mathbf{H} , H_z , be continuous across the wall–fluid interface, and therefore, no surface-excess magnetic force results,

$$f_z^M = 0. \tag{4.3}$$

B. Viscous force

The viscous traction force is easily evaluated from the Cauchy stress, (1.10), by integration over the fluid/wall interface.^{44,45} The resulting viscous force per unit area on the upper plate, in the z -direction, is given by the xz component of the Cauchy stress,

$$\tilde{T}_{xz}(\tilde{x}=1) = \frac{\eta_e}{\eta} \frac{d\tilde{v}_z}{d\tilde{z}}(\tilde{x}=1) + 2\frac{\zeta}{\eta} \tilde{\omega}_y(\tilde{x}=1), \tag{4.4}$$

where $\tilde{T}_{xz} = T_{xz}/(\eta U/d)$. This expression is easily evaluated for the zero-spin-viscosity and nonzero-spin-viscosity solutions. The result for the zero-spin-viscosity solution is

$$\tilde{T}_{xz}(\tilde{x}=1) = \frac{1}{2} \frac{\partial \tilde{p}'}{\partial \tilde{z}} + \frac{\eta_m}{\eta} \tilde{V} + \frac{(\eta_e - \eta_m)}{2\eta} \left[\left(\frac{\mu_0 H^2}{\zeta \Omega} \right) \tilde{I}_0 \right]. \tag{4.5}$$

It is striking that this result predicts finite forces even when the magnetoviscosity η_m is zero (for which infinite flow rates are obtained from this solution). The corresponding result for the nonzero-spin-viscosity solution is

$$\begin{aligned} \tilde{T}_{xz}(\tilde{x}=1) &= \frac{1}{2} \frac{\partial \tilde{p}'}{\partial \tilde{z}} + \frac{\eta_m}{\eta} \tilde{V} + \frac{\eta_e - \eta_m}{2\eta} \left(\frac{\mu_0 H^2}{\zeta \Omega} \right) \tilde{I}_0 \\ &\quad - \frac{\eta_m (\eta_e - \eta_m)}{\eta \eta_e} \\ &\quad \times \frac{(1 - \cos \kappa)}{\kappa \sin \kappa - 2[(\eta_e - \eta_m)/\eta_e](1 - \cos \kappa)} \\ &\quad \times \left[\left(\frac{\mu_0 H^2}{\zeta \Omega} \right) \tilde{I}_0 - 2\tilde{V} \right], \end{aligned} \tag{4.6}$$

when the spin–no-slip boundary condition is used, and

$$\begin{aligned} \tilde{T}_{xz}(\tilde{x}=1) &= \frac{1}{2} \frac{\partial \tilde{p}'}{\partial \tilde{z}} + \frac{\eta_m}{\eta} \tilde{V} + \frac{\eta_e - \eta_m}{2\eta} \left(\frac{\mu_0 H^2}{\zeta \Omega} \right) \tilde{I}_0 \\ &\quad - \frac{\eta_m}{\eta} \frac{(1 - \cos \kappa)}{\kappa \sin \kappa - 2[(\eta_e - \eta_m)/\eta](1 - \cos \kappa)} \\ &\quad \times \left[\frac{\eta_e - \eta_m}{\eta} \left(\frac{\mu_0 H^2}{\zeta \Omega} \right) \tilde{I}_0 - \frac{\eta_e - \eta_m}{\eta} 2\tilde{V} \right], \end{aligned} \tag{4.7}$$

when the spin/vorticity matching solution is used. Both are dependent on the spin viscosity through κ in (3.28), as expected. They only differ in the last term of the right-hand side of each expression.

Operating under conditions for which $\kappa = n\pi$ for even n , both expressions become identical to the solution for zero-spin-viscosity (4.5). Under conditions for which $\kappa = n\pi$ for odd n , the viscous traction becomes

$$\tilde{T}_{xz}(\tilde{x}=1) = \frac{1}{2} \frac{\partial \tilde{p}'}{\partial \tilde{z}} + \frac{\eta_e}{2\eta} \left(\frac{\mu_0 H^2}{\zeta \Omega} \right) \tilde{I}_0, \tag{4.8}$$

when the spin–no-slip boundary condition is used, and

$$\begin{aligned} \tilde{T}_{xz}(\tilde{x}=1) &= \frac{1}{2} \frac{\partial \tilde{p}'}{\partial \tilde{z}} + \frac{1}{2} \left[\frac{\eta_e}{\eta} + \frac{\eta_m \zeta}{\eta^2} \right] \left(\frac{\mu_0 H^2}{\zeta \Omega} \right) \tilde{I}_0 \\ &\quad + \frac{\zeta}{(\eta_e - \eta_m)} \left(\frac{\eta_m}{\eta} \right)^2 \tilde{V}, \end{aligned} \tag{4.9}$$

when the spin/vorticity matching boundary condition is used. These two expressions differ fundamentally from each other in their dependence on the velocity of the moving plate. The spin–no-slip force under these conditions is independent of the upper plate velocity \tilde{V} , whereas the spin/vorticity matching solution is not. These two expressions also differ from the corresponding result for the zero-spin-viscosity solution of (4.5) for nonzero values of the effective viscosity. As such, experiments with $\kappa = n\pi$ with odd n could be used to discern between the spin–no-slip and spin/vorticity matching boundary conditions.

Operating under conditions where $\eta_m = 0$ we obtain for the nonzero-spin-viscosity solution,

$$\begin{aligned} \tilde{T}_{xz}(\tilde{x}=1) &= \frac{1}{2} \frac{\partial \tilde{p}'}{\partial \tilde{z}} + \frac{\eta_e}{2\eta} \left(\frac{\mu_0 H^2}{\zeta \Omega} \right) \tilde{T}_0 \\ &\quad - \frac{3}{2} \left(\frac{\eta'}{\zeta d^2} \right) \frac{\eta_e^2}{\eta \zeta + 4 \eta \eta_e (\eta' / \zeta d^2)} \\ &\quad \times \left[\left(\frac{\mu_0 H^2}{\zeta \Omega} \right) \tilde{T}_0 - 2 \tilde{V} \right], \end{aligned} \tag{4.10}$$

when the spin–no-slip boundary condition is used, and

$$\begin{aligned} \tilde{T}_{xz}(\tilde{x}=1) &= \frac{1}{2} \frac{\partial \tilde{p}'}{\partial \tilde{z}} + \frac{\eta_e}{2\eta} \left(\frac{\mu_0 H^2}{\zeta \Omega} \right) \tilde{T}_0 \\ &\quad - \frac{3}{2} \left(\frac{\eta'}{\zeta d^2} \right) \frac{\eta_e^2}{\zeta \eta + 3 \eta_e^2 (\eta' / \zeta d^2)} \\ &\quad \times \left[\frac{\eta_e}{\eta} \left(\frac{\mu_0 H^2}{\zeta \Omega} \right) \tilde{T}_0 - 2 \tilde{V} \right], \end{aligned} \tag{4.11}$$

when the spin/vorticity matching boundary condition is used. Again, these two expressions differ from each other in the last term of the right-hand side.

If we consider an experiment where there is no pressure gradient ($\partial \tilde{p}' / \partial \tilde{z} = 0$), the zeroth-order body-couple is zero ($\tilde{T}_0 = 0$), and $\eta_m = 0$ (all realizable experimental conditions in principle), an experimenter neglecting the effects of spin diffusion, using (4.5), would expect that no force is required to move the plate. However, (4.10) clearly shows that non-zero spin viscosities result in a nonzero force of

$$\tilde{T}_{xz}(\tilde{x}=1) = \frac{3}{\eta} \left(\frac{\eta'}{\zeta d^2} \right) \frac{\eta_e^2}{\zeta + 4 \eta_e (\eta' / \zeta d^2)} \tilde{V}, \tag{4.12}$$

if the spin–no-slip boundary condition applies at the fluid/wall boundaries, and

$$\tilde{T}_{xz}(\tilde{x}=1) = 3 \left(\frac{\eta'}{\zeta d^2} \right) \frac{\eta_e^2}{\zeta \eta + 3 \eta_e^2 (\eta' / \zeta d^2)} \tilde{V}, \tag{4.13}$$

if the spin/vorticity matching boundary condition applies. For small values of the spin-viscosity, both expressions (that for the spin–no-slip boundary condition and that for the spin/vorticity matching boundary condition) yield

$$\lim_{\eta' / \zeta d^2 \rightarrow 0} \tilde{T}_{xz}(\tilde{x}=1) = \frac{3 \eta_e^2}{\eta \zeta} \left(\frac{\eta'}{\zeta d^2} \right) \tilde{V} + O \left[\left(\frac{\eta'}{\zeta d^2} \right)^2 \right]. \tag{4.14}$$

Using this expression, a series of experiments with ferrofluids of known vortex viscosity ζ would provide η' independent of which boundary condition applies at the ferrofluid/wall boundary. These experiments would consist of measuring the required force to move the plate at various given velocities under conditions of zero pressure gradient, zeroth-order magnetic couple and zero effective viscosity. The results of these experiments, as a curve of $\eta \zeta \tilde{T}_{xz} / 3 \eta_e^2$ vs \tilde{V} would give $\eta' / \zeta d^2$ as the slope.

Finally, suppose that the commonly accepted relationship for the vortex viscosity, equation (3.7), applies. Then we obtain for the viscous stress on the upper plate under the conditions described above in (4.13),

$$\lim_{\eta' / \zeta d^2 \rightarrow 0} \tilde{T}_{xz}(\tilde{x}=1) = \frac{4[1 + (3/2)\phi]^2}{3\phi^2} \left(\frac{\eta'}{\eta d^2} \right) \tilde{V}. \tag{4.15}$$

This last expression seems to indicate that the spin-viscosity η' has to be proportional to ϕ^2 , otherwise infinite forces would be required to move dilute suspensions (in the limit $\phi \rightarrow 0$) of ferrofluid particles. This proportionality is not immediately obvious from dimensional analysis, which indicates that $\eta' \propto \eta L^2$, with L an intrinsic length scale of the suspension (commonly assumed equal to the particle diameter).

V. DISCUSSION

The motivation of the analysis developed in this paper is to model and design experiments to determine key parameters on previously reported anomalous forward and backward ferrofluid pumping behavior in alternating and rotating magnetic fields and zero-spin-viscosity analysis that predicted multi-valued and singular flow solutions with possible zero and negative effective spin magnetoviscosity. In this paper we extend past models of plane-Poiseuille creeping flow of ferrofluids in alternating and rotating magnetic fields by including the effects of spin-diffusion and planar Couette flow. In the analysis we have calculated analytical expressions for the translational and spin-velocity profiles, vorticity profiles, volumetric flow rate, and the shear force on a moving duct surface comparing the effects of boundary conditions of zero-spin-velocity and spin-velocity equal to half the vorticity at the duct walls. This analysis shows that the single singularity in flow behavior with zero effective magnetoviscosity for the zero-spin-viscosity analysis corresponds to multiple possible flow singularities for nonzero spin-viscosity. It is hoped that near-future experiments can determine if these mathematical singularities are physical and, if so, design applications that exploit such high flow and spin velocities.

Simple representative shearing experiments have been proposed to differentiate between the zero and nonzero-spin-viscosity solutions, to calculate the values of key viscous parameters, and to show how the wall boundary conditions can be determined from shear stress measurements. We believe that a set of such similar experiments can determine all needed physical parameters which can be compared to theoretical values and scaling laws and hopefully to empirically determine the correct boundary conditions of the spin-velocity at the duct walls.

This analysis also shows the way to analyze ferrofluid flows inside and outside solid rotating cylindrical walls and in the annulus between solid rotating walls, an extension we leave to a future communication. Such geometries may be more appropriate to experimental measurements of ferrofluid shear stress on rotating cylindrical spindles. Further extensions of the planar and cylindrical analyses to nonuniform

magnetic fields offers an additional degree of freedom and perhaps stronger magnetic effects as now there can be a body force on the ferrofluid as well as a torque.

Our work only considered a duct flow with no free surfaces. Previous related work with a cylindrical flow with a top free surface³⁴ has shown that ferrofluid surface curvature can also lead to interesting flows. The effects of fluid and magnetic boundary conditions on free ferrofluid surfaces together with the bulk-driven flows of the work presented here will be the subject of future work.

Because ferrofluids are composed of nanometer scale ferromagnetic particles, there may be practical applications of magnetic-field based micro- and nano-electromechanical system (MEMS/NEMS) devices using nanometer sized ferromagnetic particles with and without carrier fluid such as for nanoduct flows, nanomotors, nanogenerators, nanopumps, nanoactuators, and other similar nanoscale devices.⁴⁰

ACKNOWLEDGMENTS

The authors are indebted to Professor Howard Brenner, of the Department of Chemical Engineering at the Massachusetts Institute of Technology, and Dr. Ronald E. Rosensweig for their encouragement and stimulating discussions on this work. This work has been supported by the US National Science Foundation Grant No. CTS-0084070. C.R. has been supported by a National Science Foundation Graduate Research Fellowship.

- ¹M. I. Shliomis, "Effective viscosity of magnetic suspensions," *Sov. Phys. JETP* **34**, 1291 (1972).
- ²M. I. Shliomis, "Nonlinear effects in a suspension of ferromagnetic particles under the influence of a rotating magnetic field," *Sov. Phys. Dokl.* **19**, 686 (1975).
- ³M. I. Shliomis and K. I. Morozov, "Negative viscosity of ferrofluid under alternating magnetic field," *Phys. Fluids* **6**, 2855 (1994).
- ⁴A. Zeuner, R. Richter, and I. Rehberg, "Experiments on negative and positive magnetoviscosity in an alternating magnetic field," *Phys. Rev. E* **58**, 6287 (1998).
- ⁵G. H. Calugaru, C. Cotae, R. Badescu, V. Badescu, and E. Luca, "A new aspect of the movement of ferrofluids in a rotating magnetic field," *Rev. Roum. Phys.* **21**, 439 (1976).
- ⁶M. Zahn and P. N. Wainman, "Effects of fluid convection and particle spin on ferrohydrodynamic pumping in traveling wave magnetic fields," *J. Magn. Magn. Mater.* **122**, 323 (1993).
- ⁷M. Zahn and D. R. Greer, "Ferrohydrodynamic pumping in spatially uniform sinusoidally time-varying magnetic fields," *J. Magn. Magn. Mater.* **149**, 165 (1995).
- ⁸M. Zahn and L. L. Pioch, "Magnetizable fluid behavior with effective positive, zero or negative dynamic viscosity," *Indian J. Eng. Mat. Sci.* **5**, 400 (1998).
- ⁹M. Zahn and L. L. Pioch, "Ferrofluid flows in ac and traveling wave magnetic fields with effective positive, zero or negative dynamic viscosity," *J. Magn. Magn. Mater.* **201**, 144 (1999).
- ¹⁰J. S. Dahler and L. E. Scriven, "Angular momentum of continua," *Nature (London)* **192**, 36 (1961).
- ¹¹J. S. Dahler and L. E. Scriven, "Theory of structured continua I. General consideration of angular momentum and polarization," *Proc. R. Soc. London, Ser. A* **276**, 504 (1963).
- ¹²H. Brenner, "Rheology of two-phase systems," *Annu. Rev. Fluid Mech.* **2**, 137 (1970).
- ¹³R. E. Rosensweig, "On magnetorheology and electrorheology as states of unsymmetric stress," *J. Rheol.* **39**, 179 (1995).
- ¹⁴R. E. Rosensweig, *Ferrohydrodynamics* (Dover, New York, 1997).
- ¹⁵B. U. Felderhof and H. J. Kroh, "Hydrodynamics of magnetic and dielec-

tric fluids in interaction with the electromagnetic field," *J. Chem. Phys.* **110**, 7403 (1999).

¹⁶It is important to note that in the general theory of structured continua (Ref. 11) the spin field ω does not strictly represent an average of the subcontinuum particle rotation rates. It is merely the proportionality factor in the defining equation

$$\langle \kappa_p \cdot \omega_p \rangle \stackrel{\text{def.}}{=} \langle \kappa_p \rangle \cdot \omega,$$

where $\langle \kappa_p \cdot \omega_p \rangle$ is a suitable ensemble average of the particle angular momenta and $\langle \kappa_p \rangle$ is a suitable ensemble average of the moment-of-inertia tensors of the subcontinuum particles.

- ¹⁷H. Brenner, "Rheology of a dilute suspension of dipolar spherical particles in an external field," *J. Colloid Interface Sci.* **32**, 141 (1970).
- ¹⁸H. Brenner and M. H. Weissman, "Rheology of a dilute suspension of dipolar spherical particles in an external field II. Effects of rotary Brownian motion," *J. Colloid Interface Sci.* **41**, 499 (1972).
- ¹⁹D. W. Condiff and J. S. Dahler, "Fluid mechanical aspects of antisymmetric stress," *Phys. Fluids* **7**, 842 (1964).
- ²⁰H. Brenner and A. Nadim, "The Lorentz reciprocal theorem for micropolar fluids," *J. Eng. Math.* **30**, 169 (1996).
- ²¹W. M. Deen, *Analysis of Transport Phenomena* (Oxford University Press, New York, 1998).
- ²²P. Brunn, "Velocity slip of polar fluids," *Rheol. Acta* **14**, 1039 (1975).
- ²³H. Lamb, *Hydrodynamics* (Dover, New York, 1945).
- ²⁴H. Brenner, "Antisymmetric stresses induced by the rigid-body rotation of dipolar suspensions—Vortex flows," *Int. J. Eng. Sci.* **22**, 645 (1984).
- ²⁵S. C. Cowin, "Note on predictions from polar fluid theory which are independent of spin boundary-condition," *Trans. Soc. Rheol.* **20**, 195 (1976).
- ²⁶K. A. Kline, "Predictions from polar fluid theory which are independent of spin boundary-condition," *Trans. Soc. Rheol.* **19**, 139 (1975).
- ²⁷K. A. Kline, "Discussion of predictions from polar fluid theory which are independent of spin boundary-conditions," *J. Rheol.* **26**, 317 (1982).
- ²⁸E. L. Aero, A. N. Bulygin, and E. V. Kuvshinski, "Asymmetric hydromechanics," *J. Appl. Math. Mech.* **29**, 333 (1965).
- ²⁹P. Brunn, "The general solution to the equations of creeping motion of a micro-polar fluid and its application," *Int. J. Eng. Sci.* **20**, 575 (1982).
- ³⁰Similar arguments apply with regards the introduction of three temporal scales in the equations that follow.
- ³¹This is with the exception of the term $\nabla \times \tilde{\omega}$ which is of order $O(L_v/L_\omega)$, with L_ω the characteristic length scale of spatial variations in ω , as introduced below.
- ³²The same comments apply to the term $\nabla \times \tilde{v}$ here as to the corresponding term $\nabla \times \tilde{\omega}$ in Eq. (1.24). The term $\nabla \times \tilde{v}$ is of $O(L_\omega/L_v)$.
- ³³V. M. Zaitsev and M. I. Shliomis, "Entrainment of ferromagnetic suspension by a rotating field," *J. Appl. Mech. Tech. Phys.* **10**, 696 (1969).
- ³⁴R. E. Rosensweig, J. Popplewell, and R. J. Johnston, "Magnetic fluid motion in rotating field," *J. Magn. Magn. Mater.* **85**, 171 (1990).
- ³⁵P. N. Kaloni, "Some remarks on the boundary-conditions for magnetic fluids," *Int. J. Eng. Sci.* **30**, 1451 (1992).
- ³⁶Note that if $\tilde{H}_z = 0$, $\tilde{B}_x = 1$.
- ³⁷The discrepancy between the constant coefficient in this relation and that given by Brenner (Ref. 12) is due to our use of a different numerical convention in the constitutive form of the stress field (1.10).
- ³⁸This may be done by making one of the two imposed fields \tilde{B}_x or \tilde{H}_z as small as necessary. This makes the product $[\tilde{B}_x^* \tilde{H}_z]$ small while α remains finite.
- ³⁹R. B. Bird, W. E. Stewart, and E. N. Lightfoot, *Transport Phenomena* (Wiley, New York, 1960).
- ⁴⁰M. Zahn, "Magnetic fluid and nanoparticle applications to nanotechnology," *J. Nanoparticle Res.* **3**, 73 (2001).
- ⁴¹R. E. Rosensweig and R. J. Johnston, "Aspects of magnetic fluid flow with nonequilibrium magnetization," in *Continuum Mechanics and its Applications*, edited by C. A. C. Graham and S. K. Malik (Hemisphere, New York, 1989), pp. 707–729.

⁴²H. Brenner and D. A. Edwards, *Macrotransport Processes* (Butterworth-Heinemann, Stoneham, MA, 1993).

⁴³J. R. Melcher, *Continuum Electromechanics* (MIT Press, Cambridge, MA, 1981).

⁴⁴Note that the Cauchy stress, in contrast with the “Maxwell stress” introduced above, is a true continuum-mechanical stress, yielding the force

exerted by a fluid on one side of a given surface on the fluid directly opposite it by integration over the open surface dividing the fluid regions, whereas the Maxwell stress yields physically meaningful forces only after integration over closed surfaces (Ref. 45).

⁴⁵C. Rinaldi and H. Brenner, “Surface vs body forces in continuum mechanics: Is the Maxwell stress tensor a physically-objective cauchy stress?” *Phys. Rev. E* **65**, 036615 (2002).